



Molybdenum(VI) complexes with ligands derived from 5-(2-pyridyl)-2H-tetrazole as catalysts for the epoxidation of olefins

Martinique S. Nunes^a, Ana C. Gomes^a, Patrícia Neves^a, Ricardo F. Mendes^a, Filipe A. Almeida Paz^a, André D. Lopes^b, Martyn Pillinger^{a,*}, Isabel S. Gonçalves^a, Anabela A. Valente^{a,*}

^a CICECO - Aveiro Institute of Materials, Department of Chemistry, University of Aveiro, Campus Universitário de Santiago, 3810-193 Aveiro, Portugal

^b CCMar, and Department of Chemistry and Pharmacy, FCT, University of the Algarve, 8005-039 Faro, Portugal

ARTICLE INFO

Keywords:

Molybdenum
Pyridyl-tetrazole ligands
Lindqvist anion
Epoxidation
Bio-olefins
Ionic liquids

ABSTRACT

The development of effective catalytic epoxidation processes that are an alternative to stoichiometric non-selective oxidation routes is important to meet environmental sustainability goals. In this work, molybdenum (VI) compounds bearing 5-(2-pyridyl)-2H-tetrazole derivatives as organic components, namely the ionic and neutral mononuclear complexes (H₂ptz)[MoO₂Cl₂(ptz)] (**1**) and [MoO₂Cl₂(tBu-ptz)] (**2**), and the new Lindqvist-type polyoxometalate (POM) [tBu-Hptz]₂[Mo₆O₁₉] (**3**), where Hptz = 5-(2-pyridyl)tetrazole and tBu-ptz = 2-*tert*-butyl-5-(2-pyridyl)-2H-tetrazole, were studied as epoxidation catalysts using readily available and relatively ecofriendly hydroperoxide oxidants, namely hydrogen peroxide and *tert*-butyl hydroperoxide (TBHP). The prepared catalysts were very active. For example, 100% *cis*-cyclooctene conversion and 100% epoxide selectivity were reached at 1 h for **1** and **3**, and 10 min for **2** (with TBHP). Catalytic and characterization studies indicated that the mononuclear complexes suffered chemical transformations under the reaction conditions, whereas **3** was structurally stable. This POM acted as a homogeneous catalyst and could be recycled by employing an ionic liquid solvent. The POM can be synthesized from **2** under different conditions, including those used in the catalytic process. Moreover, **3** was an effective epoxidation catalyst for a biobased substrate scope that included fatty acid methyl esters and the terpene *dl*-limonene.

1. Introduction

Molybdenum(VI) dioxo and oxo(diperoxo) complexes have, for several decades, been explored as catalysts for oxidation reactions [1–6]. Regarding mononuclear dioxomolybdenum(VI) complexes of the type [MoO₂X₂(L)_n] (X = halide, NCS, OR, OSiR₃, alkyl; L = mono- or bidentate ligand), the first comprehensive study was that performed by Cole-Hamilton and co-workers, who found that the complexes [MoO₂Cl₂(L)], where L is a β-ketophosphonate derived from camphor, were highly effective catalysts for the epoxidation of a wide range of alkenes, including polymeric alkenes, using *tert*-butyl hydroperoxide (TBHP) as oxidant [7–10]. Shortly thereafter, in the mid-1990's, Arnaiz *et al.* [11] and Arzoumanian *et al.* [12] reported the high activity of [MoO₂Cl₂(DMSO)₂] (DMSO = dimethylsulfoxide) and [MoO₂X₂(di-*t*-Bu-bipy)₂] (X = Br, NCS; di-*t*-Bu-bipy = 4,4'-di-*tert*-butyl-2,2'-bipyridine) as oxygen atom transfer agents towards phosphines, alcohols and arylalkanes under stoichiometric and catalytic conditions, using DMSO as

the oxygen atom source. A later development by Jeyakumar and Chand was the selective aerobic oxidation of benzylic alcohols to the corresponding carbonyls using catalytic amounts of the solvent adducts [MoO₂Cl₂(L)₂] (L = DMSO, DMF, THF) in refluxing acetonitrile [13]. Beyond the oxidation of alkenes, phosphines, alcohols and arylalkanes, the reaction scope of [MoO₂X₂(L)_n] oxidation catalysts extends to the oxidation of thiols to disulfides in DMSO [14], and the oxidation of sulfides to sulfoxides and/or sulfones using H₂O₂ as oxidant [15], with the latter reaction being applied to the oxidative desulfurization of diesel fuel containing (di)benzothiophene derivatives [16–19].

Despite the wide reaction scope for [MoO₂X₂(L)_n]-catalyzed oxidations, the epoxidation of olefins is by far the most studied transformation. Following the groundbreaking work of Cole-Hamilton and co-workers [7–10], Kühn, Romão and co-workers surveyed the performance of complexes [MoO₂X₂(L)_n] in catalytic olefin epoxidation, starting with the moisture sensitive solvent adduct [MoO₂Br₂(NCMe)₂] [20], and then expanding to complexes with different X (Cl, Br, alkyl)

* Corresponding authors.

E-mail addresses: mpillinger@ua.pt (M. Pillinger), atav@ua.pt (A.A. Valente).

<https://doi.org/10.1016/j.cattod.2023.114273>

Received 6 April 2023; Received in revised form 31 May 2023; Accepted 23 June 2023

Available online 26 June 2023

0920-5861/© 2023 The Author(s). Published by Elsevier B.V. This is an open access article under the CC BY-NC-ND license (<http://creativecommons.org/licenses/by-nc-nd/4.0/>).

and L (mono- or bidentate N,O-donor ligand) [21–24]. Taking the complex $[\text{MoO}_2\text{Cl}_2(\text{bipy})]$ as a starting point (bipy = 2,2'-bipyridine), which is appropriate since bipy is the most well studied chelating heterocyclic ligand, three avenues can be pursued to modify the catalytic performance: replace Cl by a different anionic ligand, add substituents on the bipy ligand, replace one of the pyridine ligands by a different functionality such as an imine group ($>\text{C}=\text{NR}$, R H) or azole (e.g., pyrazole, triazole, tetrazole). Adding alkoxy-carbonyl substituents in different positions on the bipy ligand greatly improved the solubility and, consequently, the catalytic performance of the complexes [25]. Replacing one of the pyridine groups in $[\text{MoO}_2\text{Cl}_2(\text{bipy})]$ by a pyrazole group (to give the ligand 2-[3(5)-pyrazolyl]pyridine (pzpy)) led to a modest increase in catalytic activity [26,27], although the catalytic performance could be enhanced further by adding n-alkyl or ethyl acetate N-substituents on the pyrazole ring [28].

While exploiting ligand effects on solubility may be the most effective way to “unleash” the catalytic potential of $[\text{MoO}_2\text{Cl}_2(\text{L})_n]$ complexes, catalytic behavior may also be directly impacted by the ligands' electronic and steric properties, which may influence the Lewis acidity of the metal center, and other physicochemical properties such as thermal stability and moisture sensitivity. Ligand effects go beyond the modification of catalytic behavior, e.g., when the dichloro complexes are deliberately hydrolyzed by treating them with water, the organic ligand L plays a structure-directing role regarding the nature of the molybdenum oxide (MOXI)-ligand hybrid material formed. This is amply demonstrated by results obtained for the complexes mentioned above. The reaction of $[\text{MoO}_2\text{Cl}_2(\text{bipy})]$ with water gives $\{[\text{MoO}_3(2,2'\text{-bipy})][\text{MoO}_3(\text{H}_2\text{O})]\}_n$ with a structure containing alternating one-dimensional (1D) inorganic and organic-inorganic polymers [26], while hydrolysis of $[\text{MoO}_2\text{Cl}_2(\text{di-}t\text{Bu-bipy})_2]$ gives the octanuclear complex $[\text{Mo}_8\text{O}_{22}(\text{OH})_4(\text{di-}t\text{Bu-bipy})_4]$ [29]. For the pyrazolylpyridine complexes $[\text{MoO}_2\text{Cl}_2(\text{L})]$ with L = pzpy or ethyl[3-(pyridin-2-yl)-1H-pyrazol-1-yl]acetate, hydrolysis leads to structurally distinct MOXI materials formulated as $[\text{Mo}_3\text{O}_9(\text{pzpy})]_n$ [27] and $[\text{Mo}_2\text{O}_6(\text{HpypzA})]$ (HpypzA = [3-(pyridinium-2-yl)-1H-pyrazol-1-yl]acetate) [30], respectively. The interesting catalytic behavior displayed by these compounds, e.g., in the epoxidation of olefins [26,27,29,30], the oxidation of secondary amines to nitrones [31], and oxidative desulfurization/denitrogenation [32], encourages further study of complexes of the type $[\text{MoO}_2\text{Cl}_2(\text{L})_n]$ as synthetic precursors to the family of catalytically useful MOXI materials.

We recently described the synthesis and crystal structure of the complex salt $(\text{H}_2\text{ptz})[\text{MoO}_2\text{Cl}_2(\text{ptz})]$ (**1**) (Hptz = 5-(2-pyridyl)tetrazole), and its hydrolysis to give a MOXI hybrid material formulated as $[\text{MoO}_3(\text{Hpytz})]$ [33]. Although the crystal structure of the hybrid was not determined, the material was interesting because, while **1** behaved as a homogeneous catalyst in the epoxidation of *cis*-cyclooctene (Cy) with TBHP, the hybrid could be used as a recyclable heterogeneous catalyst, and the substrate scope was broadened to include bio-based olefins (*dl*-limonene and fatty acid methyl esters (FAMES)), which gave predominantly epoxide products. In the present work, we have carried out a parallel study, aiming to evaluate the effect of adding a *tert*-butyl N-substituent on the tetrazole group. This has resulted in the synthesis of the neutral complex $[\text{MoO}_2\text{Cl}_2(t\text{Bu-ptz})]$ (**2**) (*t*Bu-ptz = 2-*tert*-butyl-5-(2-pyridyl)-2H-tetrazole) and the polyoxometalate (POM) salt $[t\text{Bu-Hptz}]_2[\text{Mo}_6\text{O}_{19}]$ (**3**) (*t*Bu-Hptz = 2-*tert*-butyl-5-(2-pyridinium)-2H-tetrazole). We describe a comparison of **1-3** as catalysts in the epoxidation of Cy, the crystal structure of **3**, confirmation that **3** is formed in situ from **2** under the catalytic reaction conditions, and extension of the substrate scope to bio-based olefins.

2. Experimental

2.1. Synthesis

2.1.1. Methods and materials

The following reagents and chemicals were purchased from Sigma-Aldrich, unless indicated otherwise, and used as received: perchloric acid (Honeywell, 70%), *tert*-butanol (> 99.3%), 1 M sodium hydroxide (Honeywell), molybdenum(VI) dichloride dioxide, anhydrous tetrahydrofuran ($\geq 99.9\%$), hexane ($\geq 99\%$, Carlo Erba), and anhydrous diethyl ether ($\geq 99.8\%$, Honeywell). All air-sensitive operations were carried out using standard Schlenk techniques under a nitrogen atmosphere. The complex $(\text{H}_2\text{ptz})[\text{MoO}_2\text{Cl}_2(\text{ptz})]$ (**1**) and 5-(2-pyridyl)tetrazole (Hptz) were prepared as described previously [33].

2.1.2. 2-*tert*-Butyl-5-(2-pyridyl)-2 H-tetrazole (*t*Bu-ptz)

The preparation of *t*Bu-ptz was based on the procedure described by Mosalkova et al. [34]. *tert*-Butanol (2.3 mL, 7.00 mmol) was added dropwise with stirring to a suspension of Hptz (1.03 g, 7.00 mmol) in 70% aqueous perchloric acid (2.3 mL). The colorless solution was stirred at room temperature for 2 h and then neutralized with 1 M NaOH to pH 7–8. The resultant white precipitate was filtered, washed with cold water (10×10 mL), and vacuum-dried. Yield: 0.93 g, 65%. Satisfactory elemental analyses were obtained, and the FT-IR and ^1H NMR data agreed with published spectra [34–36]. Raman (cm^{-1}): $\nu = 3060$ (w), 2997 (w), 2938 (w), 2916 (w), 1594 (vs), 1573 (m), 1522 (vs), 1458 (m), 1382 (w), 1203 (w), 1172 (w), 1153 (w), 1055 (w), 1020 (m), 992 (s), 826 (w), 624 (w), 294 (w), 272 (w), 167 (w). ^1H NMR (500.16 MHz, 25 °C, DMSO- d_6): $\delta = 8.74$ (ddd, 1H, $J_{\text{H-H}} = 4.8, 1.8, 1.0$ Hz, H6), 8.15 (dt, 1H, $J_{\text{H-H}} = 7.7, 1.0$ Hz, H3), 8.01 (td, 1H, $J_{\text{H-H}} = 7.7, 1.8$ Hz, H4), 7.55 (ddd, 1H, $J_{\text{H-H}} = 7.7, 4.8, 1.0$ Hz, H5), 1.76 (s, 9H, *t*Bu) ppm. ^{13}C $\{^1\text{H}\}$ NMR (125.76 MHz, 25 °C, DMSO- d_6): $\delta = 163.7$ (Ctz), 150.1 (C6), 146.5 (C2), 137.6 (C4), 125.2 (C5), 122.4 (C3), 64.2 (C_{ipso}), 29.0 (*t*Bu) ppm.

2.1.3. 2-*tert*-Butyl-5-(2-pyridinium)-2 H-tetrazole chloride (*t*Bu-Hptz) Cl

3 M HCl (0.82 mL, 2.46 mmol, 5 equiv.) was added dropwise with stirring to a suspension of *t*Bu-ptz (0.10 g, 0.49 mmol) in water (1 mL). The mixture was stirred at room temperature for 20 min. After evaporating the resultant clear solution to dryness under reduced pressure, the desired salt was obtained in quantitative yield. FT-IR (KBr, cm^{-1}): $\nu = 3313$ (m), 2991 (w), 1633 (m), 1553 (w), 1472 (m), 1376 (w), 1297 (w), 1254 (w), 1196 (w), 1147 (w), 973 (w), 797 (s), 761 (s), 718 (m), 615 (w), 592 (w), 523 (w), 443 (w), 400 (w). Raman (cm^{-1}): $\nu = 3103$ (m), 3086 (m), 2989 (m), 2933 (m), 1627 (vs), 1614 (m), 1553 (m), 1478 (m), 1451 (w), 1387 (w), 1300 (w), 1273 (w), 1238 (w), 1211 (w), 1165 (m), 1151 (m), 1044 (w), 1014 (s), 1003 (m), 940 (w), 826 (w), 625 (w), 293 (w), 281 (w), 167 (w), 114 (vs), 80 (s). ^1H NMR (500.16 MHz, 25 °C, D_2O): $\delta = 8.83$ (d, 1H, $J_{\text{H-H}} = 5.7$ Hz, H_{arom}), 8.64 (td, 1H, $J_{\text{H-H}} = 8.0, 1.5$ Hz, H_{arom}), 8.57 (d, 1H, $J_{\text{H-H}} = 8.0$ Hz, H_{arom}), 8.07 (ddd, 1H, $J_{\text{H-H}} = 7.3, 5.7, 1.3$ Hz, H_{arom}), 1.76 (s, 9H, *t*Bu) ppm. $^{13}\text{C}\{^1\text{H}\}$ NMR (125.76 MHz, 25 °C, D_2O): $\delta = 158.0$ (Ctz), 146.9, 143.3, 139.8, 128.0, 125.1, 66.6 (C_{ipso}), 28.4 (*t*Bu) ppm.

2.1.4. $[\text{MoO}_2\text{Cl}_2(t\text{Bu-ptz})]$ (**2**)

Anhydrous tetrahydrofuran (20 mL) was added to MoO_2Cl_2 (0.50 g, 2.52 mmol) and the mixture was stirred at 50 °C for 25 min. The ligand *t*Bu-ptz (0.51 g, 2.52 mmol) was then added and stirring continued at rt for 4 h.¹ After concentrating the solution, hexane (60 mL) was added and a white solid precipitated, which was filtered, washed with hexane (2×10 mL), and vacuum-dried. Yield: 0.87 g, 86%. Anal. Calcd for

¹ The reaction conditions were not optimized. Very good yields of **2** may be achievable with shorter reaction times (<2 h).

C₁₀H₁₃Cl₂MoN₅O₂ (402.09): C, 29.87; H, 3.26; N, 17.42. Found: C, 30.27; H, 3.44; N, 16.98%. FT-IR (KBr, cm⁻¹): $\nu = 3444$ (w, br), 3098 (w), 3063 (w), 2987 (m), 2937 (w), 1619 (s), 1574 (w), 1556 (m), 1455 (vs), 1391 (w), 1377 (m), 1308 (m), 1278 (w), 1260 (w), 1220 (m), 1194 (w), 1173 (s), 1103 (m), 1066 (m), 1050 (m), 1026 (m), 1017 (w), 948 (vs), 918 (vs), 821 (w), 803 (s), 758 (s), 729 (s), 642 (m), 599 (m), 543 (w), 516 (w), 423 (m), 376 (w). Raman (cm⁻¹): $\nu = 3098$ (w), 3066 (w), 2987 (w), 2945 (w), 2928 (w), 1619 (s), 1575 (m), 1556 (m), 1462 (w), 1392 (w), 1158 (w), 1016 (s), 947 (vs), 923 (w), 823 (w), 377 (w), 316 (w), 286 (w), 253 (w), 230 (w), 191 (w), 168 (w), 145 (s), 105 (s), 71 (s). ¹H NMR (500.16 MHz, 25 °C, CDCl₃): $\delta = 9.50$ (dt, 1H, $J_{H-H} = 5.3, 1.5$ Hz, H6), 8.33 (dt, 1H, $J_{H-H} = 7.7, 1.2$ Hz, H3), 8.20 (td, 1H, $J_{H-H} = 7.7, 1.5$ Hz, H4), 7.80 (ddd, 1H, $J_{H-H} = 7.7, 5.3, 1.2$ Hz, H5), 1.90 (s, 9H, tBu). ¹³C{¹H} NMR (125.76 MHz, 25 °C, CDCl₃): $\delta = 160.1$ (Ctz), 151.5 (C6), 141.6 (C2), 140.4 (C4), 127.8 (C5), 123.3 (C3), 68.3 (C_{ipso}), 29.4 (tBu) ppm.

2.1.5. [tBu-Hptz]₂[Mo₆O₁₉] (3)

A suspension of **2** (0.25 g, 0.62 mmol) in Milli-Q water (10 mL) was refluxed for 24 h. The resultant pale green solid was separated from the clear mother liquor (which had a low pH of 1–2 due to the presence of HCl resulting from the hydrolysis of the Mo–Cl bonds in **2**), washed with water (2 × 5 mL) and diethyl ether (2 × 5 mL), and finally vacuum-dried. Yield: 0.11 g, 83%. Single crystals suitable for X-ray diffraction were obtained by two distinct methods: slow evaporation of a concentrated solution of **3** in acetone, or by diffusion of anhydrous diethyl ether into a concentrated solution of **3** in acetone. Anal. Calcd for C₂₀H₂₈Mo₆N₁₀O₁₉ (1288.13): C, 18.65; H, 2.19; N, 10.87. Found: C, 18.82; H, 2.26; N, 10.90%. FT-IR (KBr, cm⁻¹): $\nu = 3453$ (m, br), 3162 (m), 3097 (m), 2987 (m), 1642 (s), 1618 (s), 1551 (w), 1514 (m), 1459 (s), 1397 (w), 1373 (s), 1297 (m), 1275 (w), 1238 (m), 1198 (w), 1181 (w), 1091 (w), 1055 (m), 955 (vs), 798 (s), 745 (m), 712 (w), 591 (m), 512 (w), 443 (m). Raman (cm⁻¹): $\nu = 3115$ (m), 2939 (m), 1641 (s), 1628 (w), 1520 (w), 1512 (m), 1464 (m), 1391 (w), 1307 (w), 1240 (w), 1186 (w), 1170 (w), 1155 (w), 1026 (m), 1013 (m), 987 (vs), 962 (s), 820 (w), 750 (w), 714 (w), 623 (w), 604 (w). ¹H NMR (500.16 MHz, 25 °C, acetone-*d*₆): $\delta = 9.23$ (d, 1H, $J_{H-H} = 5.8$ Hz, H_{arom}), 8.97 (m, 1H, H_{arom}), 8.90 (d, 1H, $J_{H-H} = 7.8$ Hz, H_{arom}), 8.39 (ddd, 1H, $J_{H-H} = 7.4, 5.8, 1.4$ Hz, H_{arom}), 1.86 (s, 9H, tBu) ppm.

2.2. Characterization

2.2.1. Single-crystal X-ray diffraction studies

A single crystal of **3** was manually collected from the crystallization vial and immersed in highly viscous FOMBLIN Y perfluoropolyether vacuum oil (LVAC 140/13, Sigma-Aldrich) to avoid degradation caused by the evaporation of the solvent [37]. The crystal was mounted on a MiTeGen MicroLoop with the help of a Stemi 2000 stereomicroscope equipped with Carl Zeiss lenses.

Crystal data were collected at 150(2) K on a Bruker D8 QUEST equipped with a Mo-K α sealed tube ($\lambda = 0.71073$ Å), a multilayer TRUMP X-ray mirror, and a PHOTON III CMOS detector, controlled by the APEX3 software package [38], and an Oxford Instruments 700+ Series Cryostream cooler monitored remotely using the software interface Cryopad [39]. Diffraction images were processed using SAINT+ [40] and data were corrected for absorption by the multiscan semi-empirical method implemented in SADABS 2016/2 [41].

The structure was solved using the algorithm implemented in SHELXT-2014/5 [42], which allowed the immediate location of almost all the heaviest atoms composing their molecular units. The remaining missing and misplaced non-hydrogen atoms were located from difference Fourier maps calculated from successive full-matrix least-squares refinement cycles on F^2 using the latest SHELXL from the 2018/3 release [42]. All structural refinements were performed using the graphical interface ShelXle [43].

Hydrogen atoms bonded to carbon were placed at their idealized

positions using HFIX instructions in SHELXL: 43 (for aromatic carbon atoms and -NH groups) and 137 (for the -CH₃ groups). These hydrogen atoms were included in subsequent refinement cycles with isotropic thermal displacement parameters (U_{iso}) fixed at $1.2 \times U_{eq}$ of the parent carbon atoms. The two tBu-Htpz⁺ cations present in the asymmetric unit were found to be disordered over two positions each, which were fixed in the final stages of the refinement to occupancy factors of 35% and 65%. The last difference Fourier map synthesis showed the highest peak (0.45 eÅ⁻³) and the deepest hole (-0.72 eÅ⁻³) located at 0.40 and 0.75 Å from H39C and Mo3, respectively.

Crystal data for **3**: C₂₀H₂₈Mo₆N₁₀O₁₉, $M = 1288.13$, monoclinic, space group $P2_1/c$, $Z = 4$, $a = 16.062(3)$ Å, $b = 18.395(4)$ Å, $c = 12.132(3)$ Å, $\beta = 94.978(5)^\circ$, $V = 3570.9(13)$ Å³, $\mu(\text{Mo-K}\alpha) = 2.135$ mm⁻¹, yellow block with crystal size of $0.36 \times 0.30 \times 0.30$ mm³. Of a total of 66366 reflections collected, 6290 were independent ($R_{int} = 0.0513$). Final $R1 = 0.0399$ [$I > 2\sigma(I)$] and $wR2 = 0.1046$ (all data). Data completeness to theta = 25.24°, 96.0%.

CCDC 2251524 contains the supplementary crystallographic data (including structure factors) for this paper. These data can be obtained free of charge from The Cambridge Crystallographic Data Centre via www.ccdc.cam.ac.uk/structures. Structural drawings were created using Crystal Impact Diamond [44].

2.2.2. Instrumentation

Elemental analyses (carbon, hydrogen, and nitrogen) were performed using a TruSpec 630–200–200 analyzer. Fourier transform infrared (FT-IR) spectra (in the range 350–4000 cm⁻¹) were measured on a Bruker Tensor 27 spectrophotometer (resolution 4 cm⁻¹, 128 scans) as KBr pellets. Attenuated total reflectance (ATR) FT-IR spectra were measured using a Mattson-7000 infrared spectrophotometer, with a Specac Golden Gate Mk II ATR accessory having a diamond top plate and KRS-5 focusing lenses. FT-Raman spectra were recorded on a Bruker MultiRAM spectrometer equipped with a Nd:YAG laser with an excitation wavelength of 1064 nm. Powder X-Ray diffraction (PXRD) data were collected on a Malvern Panalytical (Malvern, UK) Empyrean diffractometer (Cu-K α X-radiation, $\lambda = 1.54060$ Å; 45 kV, 40 mA) in a Bragg-Brentano *para*-focusing optics configuration at ambient temperature, using a spinning flat plate sample holder. Samples were step-scanned from 3° to 70° (2θ) with steps of 0.026°. All the NMR spectra were recorded using a 500 MHz JEOL system equipped with a Royal HFX probe.

2.3. Catalysis

2.3.1. Materials

The following reagents and chemicals were purchased from Sigma-Aldrich, unless indicated otherwise, and used as received: *cis*-cyclooctene (95%, Alfa Aesar), methyl oleate (99%), methyl linoleate (95%, Alfa Aesar), *dl*-limonene (>95%, Merck), 5.5 M TBHP in decane, 70 wt% aq. TBHP, 30 wt% aqueous H₂O₂, acetonitrile (99.9%, Panreac), anhydrous benzotrifluoride ($\geq 99\%$), ethanol (99.9%, Carlo Erba), acetone (99.5%, Honeywell, Riedel de Haen), diethyl ether (99.8%), pentane (>95%, Carlo-Erba), undecane (>99%), methyl decanoate (99%), 1-butyl-3-methylimidazolium bis(trifluoromethylsulfonyl)imide (99%, Iolitec), and 1-butyl-3-methylimidazolium tetrafluoroborate (99%, Iolitec).

2.3.2. General procedures

The catalysts were tested for the epoxidation of olefins at 55 or 70 °C, using TBHP (5.5 M solution in decane), 70 wt% aq. TBHP (TBHPaq) or H₂O₂ as oxidants, and benzotrifluoride (BZF), acetonitrile (MeCN) or the ionic liquids (ILs) 1-butyl-3-methylimidazolium bis(trifluoromethylsulfonyl)imide ([BMIM][NTf₂]) and 1-butyl-3-methylimidazolium tetrafluoroborate ([BMIM]BF₄) as solvents. The olefins were *cis*-cyclooctene (Cy), methyl oleate (OLE), methyl linoleate (LIN) and *dl*-limonene (LIM). The initial Mo:olefin:oxidant molar ratio was 1:100:153

(for Cy) and 1:100:210 for the remaining substrates.

The reactions with TBHP or TBHPaq were carried out in 10 mL borosilicate vials that were capped with a Teflon valve for sampling. The reactors were loaded with catalyst, solvent (1 mL of organic solvent or 0.3 mL of IL), olefin and PTFE-coated magnetic stirring bar, and then immersed in an oil bath set to the desired temperature, under stirring (1000 rpm) for 10 min. The oxidant was preheated in a separate flask for 10 min at the same temperature, and then added to the (heated) reactor and this moment was taken as the initial instant of the catalytic reaction.

The reactions with H₂O₂ were performed in tubular borosilicate batch reactors with pear-shaped bottoms (ca. 12 mL capacity), closed with a valve for sampling. The catalyst, substrate, MeCN, H₂O₂ and PTFE-coated magnetic bar (for stirring at 1000 rpm) were added to the reactor, which was then immersed in an oil bath set to the desired temperature, and this moment was taken as the initial instant of the catalytic reaction.

The reaction mixtures were analyzed using an Agilent 7820 A gas chromatograph equipped with a DB-5 capillary column (30 m × 0.25 mm × 0.25 μm) and a FID detector with H₂ as the carrier gas. Product quantification was based on calibrations using internal standards; undecane for the Cy and LIM reactions, and methyl decanoate for the OLE and LIN reactions. The experimental range of error was less than 6%, based on 2–3 replicates carried out for selected experimental conditions. The reaction products were identified by GC-MS (Trace GC 2000 Series Thermo Quest CE Instruments GC; Thermo-Scientific DSQ II), using He as the carrier gas. The product identifications were based on commercial mass spectrometry databases (Wiley6, NIST2.0, NIST-Chemistry WebBook, MAINLIB) and mass spectra similarities. Iodometric titration was performed to check the oxidant efficiency for 3/Cy/BZF/TBHP. The initial turnover frequency (TOF, mol mol_{Mo}⁻¹ h⁻¹) was calculated based on olefin conversion at 10 min reaction, and considering that the total amount of catalyst added to the reactor was catalytically active and that each molybdenum center played a catalytic role.

For biphasic liquid-solid reaction systems the undissolved solids were separated from the mixtures by centrifugation (5000 rpm), thoroughly washed with diethyl ether or acetone, dried at rt overnight and then at 60 °C for 1 h under vacuum (ca. 4 mbar), giving i-S-TBHP-runx, where i = 1, 2 or 3, and x is the number of the catalytic batch run (x = 1 for the catalyst recovered after the first run). The recovered solids were recycled using the same initial catalyst: Cy:TBHP mass ratio as that used in run 1. The soluble molybdenum species were isolated as follows (for 3/Cy/TBHP/70 °C): the reaction mixture was centrifuged, and the liquid phase was passed through a 0.2 μm PTFE membrane filter, and then a mixture of diethyl ether and pentane (1:2 v/v) was added to the filtrate to induce precipitation of metal-containing species at rt. The precipitated solid was washed and dried (as described above for i-S-TBHP-runx), giving 3-L-TBHP-run1. The recovered solids were characterized by ATR FT-IR spectroscopy and PXRD.

The system 3/Cy/TBHP was recycled using an IL as solvent. Between batch runs, the reaction mixtures were extracted with hexane (4 stages). Specifically, hexane was added to the reaction mixture (ca. 3:1 v/v), which was stirred at 1000 rpm for 5 min at rt, followed by centrifugation/decantation of the mixture which consisted of an upper organic phase (containing reactants/products) and a lower phase (containing IL/catalyst). The IL/catalyst mixture was vacuum-dried at 40 °C for 1 h. Cy was then added, and the mixture was preheated at 70 °C for 10 min before adding preheated TBHP.

A leaching test (LT) was carried out for 3/BZF/TBHP as follows: after 10 min reaction at 70 °C, the mixture was passed through a 0.2 μm PTFE membrane filter. The hot filtrate was transferred immediately to a separate reactor (preheated at 70 °C), and the evolution of the homogeneous phase reaction was monitored by GC as described above for normal catalytic tests.

3. Results and discussion

3.1. Catalyst synthesis and characterization

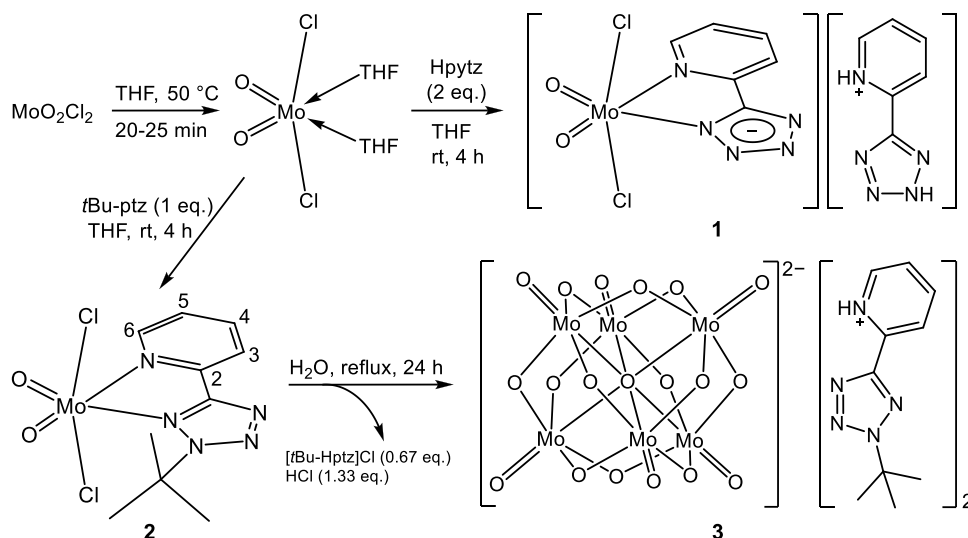
The equimolar reaction between the solvent adduct [MoO₂Cl₂(THF)₂] in THF and the ligand *t*Bu-ptz afforded [MoO₂Cl₂(*t*Bu-ptz)] (**2**) in very good yield (Scheme 1). Complex **2** is soluble in DMSO, acetone, dichloromethane and acetonitrile, insoluble in water, diethyl ether and hexane, and partially soluble in ethanol. The vibrational spectra of **2** display bands at 948–947 cm⁻¹ (very strong in the IR and in the Raman) and 918–923 cm⁻¹ (very strong in the IR, weak in the Raman), which are attributed to symmetric and asymmetric Mo=O stretching modes, respectively (Fig. 1b and Fig. 2b). The out-of-plane deformation mode, γ(MoO₂), occurs as a weak-intensity band at 376–377 cm⁻¹ in the IR and Raman. In the Raman spectrum (Fig. 2b), the ν_s(Mo-Cl) vibrational mode is assigned to the weak band at 230 cm⁻¹. These attributions are in good agreement with previous assignments made for complexes [MoO₂Cl₂(L)] containing pyrazolylpyridine ligands [28,45]. The coordination of the ligand *t*Bu-ptz to the Mo center in **2** is supported by the shift of bands in the range 1500–1600 cm⁻¹ (attributed to pyridyl C-C, pyridyl C-N, and inter-ring stretching modes) to higher frequency (1550–1620 cm⁻¹) [28,36,45]. Both the IR and the Raman spectra display the shifted bands at 1556, 1575 and 1619 cm⁻¹. Vibrational bands in the range 1350–1500 cm⁻¹ are assigned to tetrazole stretching modes [ν(C=N), ν(N=N)] [33]. A strong IR band at 1431 cm⁻¹ for *t*Bu-ptz (Fig. 1a) is evidently shifted to 1455 cm⁻¹ for **2** (Fig. 1b), which indicates that the nitrogen linked by a double bond to the tetrazolyl ring carbon takes part in complexation [46,47]. In the spectral region between 3050 and 3100 cm⁻¹, bands due to ν(CH) of the pyridine ring shift slightly to higher frequency on going from *t*Bu-ptz (3055–3060, 3087–3090 cm⁻¹) to **2** (3063–3066, 3098 cm⁻¹).

The ¹H NMR spectrum of the ligand *t*Bu-ptz in DMSO-*d*₆ shows four pyridyl ring proton signals between 7.5 and 8.8 ppm (Fig. S1 in the Supporting Information). An additional singlet is observed at 1.76 ppm for the *tert*-butyl substituent group. The corresponding aromatic signals for **2** (in CDCl₃) are shifted downfield to varying degrees (0.17–0.76 ppm) due to coordination of the ligand to the metal center in a bidentate fashion.² The large shift of 0.76 ppm occurs for H6, while smaller shifts of 0.17–0.25 ppm are observed for the other three protons. The unambiguous assignment of the ¹H and ¹³C NMR spectra of **2** was achieved by recording a ¹H-¹³C HSQC NMR spectrum (Fig. S2 in the Supporting Information).

The reaction of **2** in refluxing water for 24 h led to the isolation of the POM hybrid salt [tBu-Hptz]₂[Mo₆O₁₉] (**3**) in very good yield (Scheme 1). Single crystals of **3** suitable for crystallographic study were obtained from solutions of the salt in acetone.

Compound **3** crystallizes in the centrosymmetric space group P2₁/c with the asymmetric unit containing an anionic polyoxometalate ([Mo₆O₁₉]²⁻), commonly known as a Lindqvist super octahedron, and two 2-*tert*-butyl-5-(2-pyridinium)-2H-tetrazole cations. Both [tBu-Hptz]⁺ cations act as counterions, each being disordered with refined occupancy factors of 35% and 65% (Fig. 3). The [Mo₆O₁₉]²⁻ anion is typical, being composed of six molybdenum and 19 oxygen atoms, with each cation exhibiting a distorted octahedral coordination sphere. The average bond lengths for the Mo-O_t (terminal oxygen), Mo-O_c (center oxygen) and Mo-O_b (bridging oxygen) are 1.68, 2.32 and 1.93 Å, respectively. These values agree well with the structural features

² An inert non-coordinating solvent (CDCl₃) was favored for the NMR study of **2** to guarantee the absence of ligand exchange phenomena. A same-solvent comparison with *t*Bu-ptz is not possible since the pure ligand is not soluble in CDCl₃. The association of the downfield shifts with ligand coordination (rather than a solvent effect) was made considering that δ(DMSO)-δ(CDCl₃) solvent shifts for the aromatic protons are not expected to be greater than ca. ± 0.1 ppm [48].



Scheme 1. Preparation and structures of compounds 1–3 studied in this work. The structure of **2** shows the pyridyl carbon atom numbering for the NMR assignments of *t*Bu-ptz and **2**.

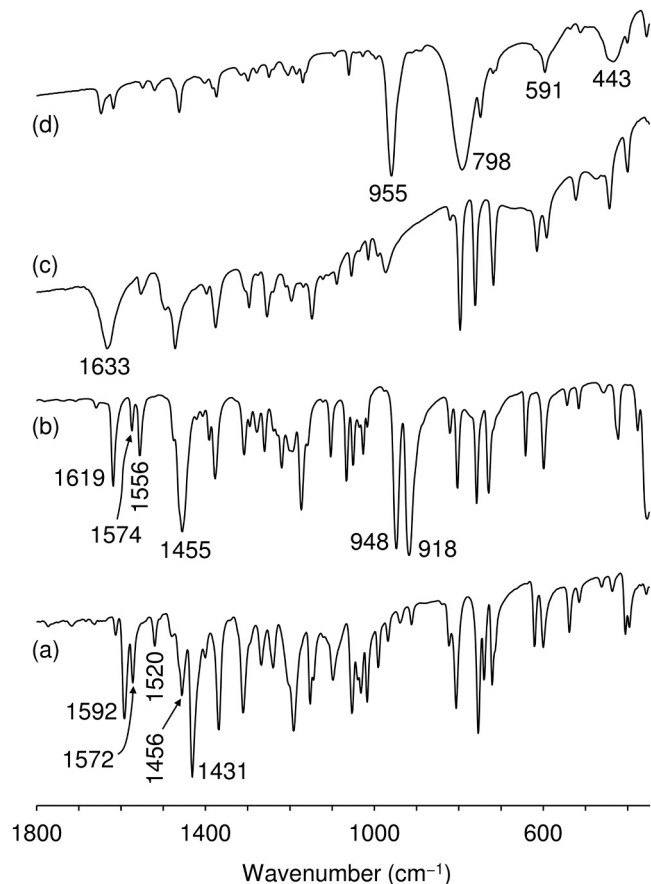


Fig. 1. FT-IR spectra in the range $350\text{--}1850\text{ cm}^{-1}$ of (a) ligand *t*Bu-ptz, (b) complex **2**, (c) $[\text{tBu-Hptz}]\text{Cl}$, and (d) POM hybrid salt **3**.

reported in the CCDC database for this type of Lindqvist super octahedron ($d_{\text{Mo}\cdots\text{O}}$ between 1.622 and 2.581 Å).

The crystal packing of **3** is essentially mediated by several cooperative weak hydrogen bonding interactions. The $[\text{Mo}_6\text{O}_{19}]^{2-}$ anion is “trapped” between pairs of disordered $[\text{tBu-Hptz}]^+$ cations in a “sandwich”-type fashion along the [101] direction of the unit cell (Fig. 4a), maintained by weak C-H \cdots O hydrogen bonding interactions. The

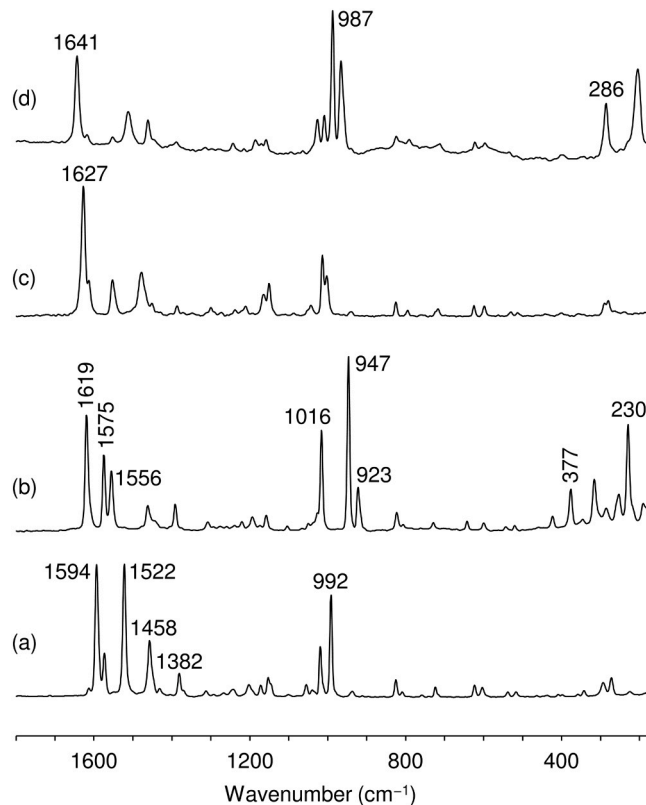


Fig. 2. FT-Raman spectra in the range $200\text{--}1850\text{ cm}^{-1}$ of (a) ligand *t*Bu-ptz, (b) complex **2**, (c) $[\text{tBu-Hptz}]\text{Cl}$, and (d) POM hybrid salt **3**.

disordered $[\text{tBu-Hptz}]^+$ cations fill the space between the anionic POMs as supramolecular pairs of charged molecules (Fig. 4b), interconnected by strong $\text{N}^+\text{--H}\cdots\text{O}$ hydrogen bonding interactions between a pyridinium group and the symmetry related tetrazole ring ($d_{\text{N}\cdots\text{N}} = 2.83$ (2)–2.854(14) Å with $\angle\text{NHN}$ interaction angles between 156° and 159°).

Having determined the crystal structure of **3**, the phase purity of the bulk as-synthesized material was confirmed by the good match between the experimental and calculated PXRD patterns (Fig. 5). The FT-IR spectrum of **3** displays the characteristic bands for the Lindqvist

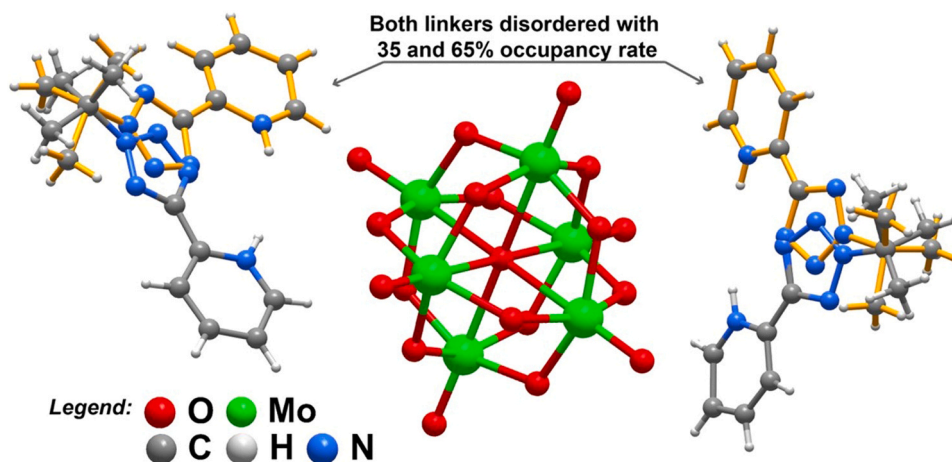


Fig. 3. Asymmetric unit of compound $[t\text{Bu-Hptz}]_2[\text{Mo}_6\text{O}_{19}]$ (**3**) emphasizing the disorder of both symmetry-independent $[t\text{Bu-Hptz}]^+$ cations.

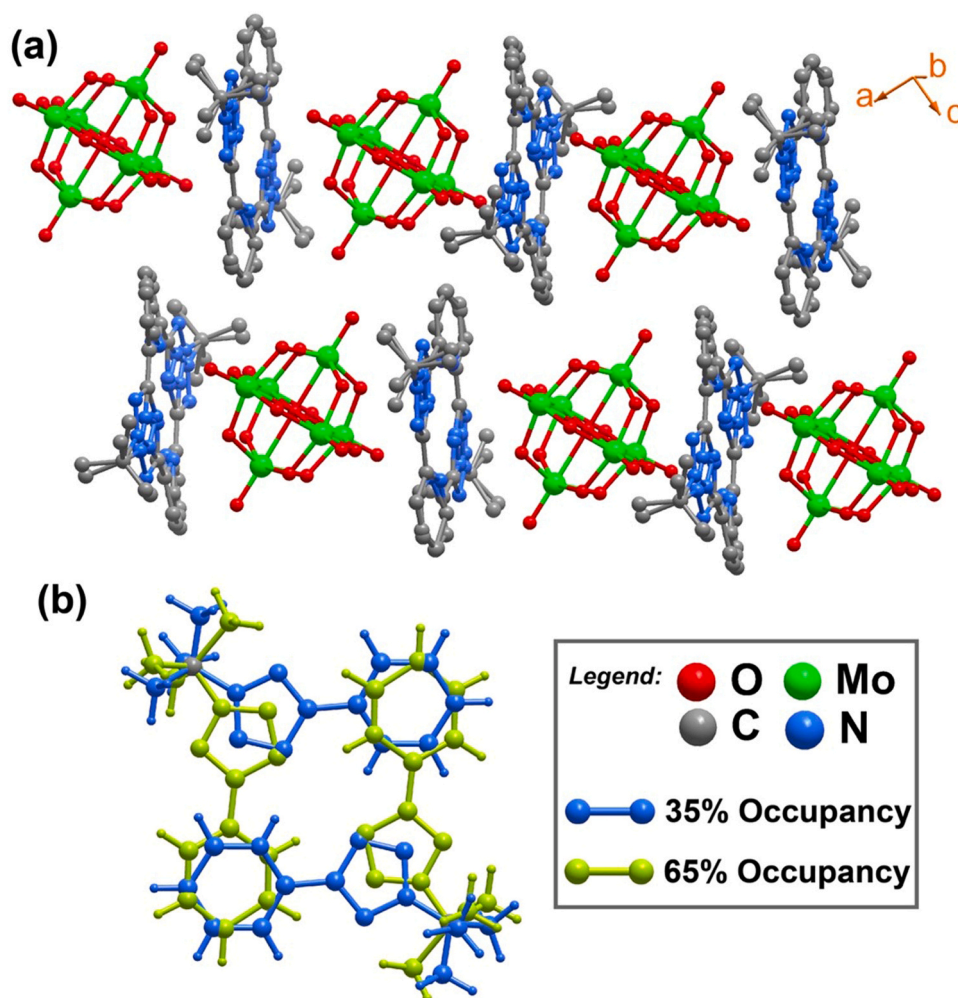


Fig. 4. (a) Schematic representation of the crystal packing of $[t\text{Bu-Hptz}]_2[\text{Mo}_6\text{O}_{19}]$ (**3**) (hydrogen atoms have been omitted for clarity). (b) Detail view of the disordered symmetry-related $[t\text{Bu-Hptz}]^+$ cations that occupy the “free” space between individual $[\text{Mo}_6\text{O}_{19}]^{2-}$ anions.

polyanion, namely very strong bands at 955 cm^{-1} ($\nu_{\text{as}}(\text{Mo}-\text{O}_t)$) and 798 cm^{-1} ($\nu_{\text{as}}(\text{Mo}-\text{O}_b)$), and medium-intensity bands at 591 and 443 cm^{-1} ($\delta(\text{O}_b-\text{Mo}-\text{O}_t)$ or $\delta(\text{O}_b-\text{Mo}-\text{O}_t) + \nu_{\text{as}}(\text{Mo}-\text{O}_b)$) [49]. In the Raman spectrum, the $\nu_s(\text{Mo}-\text{O}_t)$ mode appears as a strong band at 987 cm^{-1} , and the medium-intensity band at 286 cm^{-1} is assigned to $\nu_s(\text{Mo}-\text{O}_b)$.

To characterize **3** further, the salt $[t\text{Bu-Hptz}]\text{Cl}$ was prepared. Protonation of the nitrogen atom of the pyridyl ring in $t\text{Bu-ptz}$ resulted in a shift of the pyridyl ring stretching absorption band from $1592\text{--}1594\text{ cm}^{-1}$ to $1627\text{--}1633\text{ cm}^{-1}$ in the IR and Raman spectra (Figs. 1 and 2). Comparing the ^1H NMR spectra of $t\text{Bu-ptz}$ (in $\text{DMSO-}d_6$) and $[t\text{Bu-Hptz}]\text{Cl}$ (in D_2O), the four pyridyl ring proton signals shift

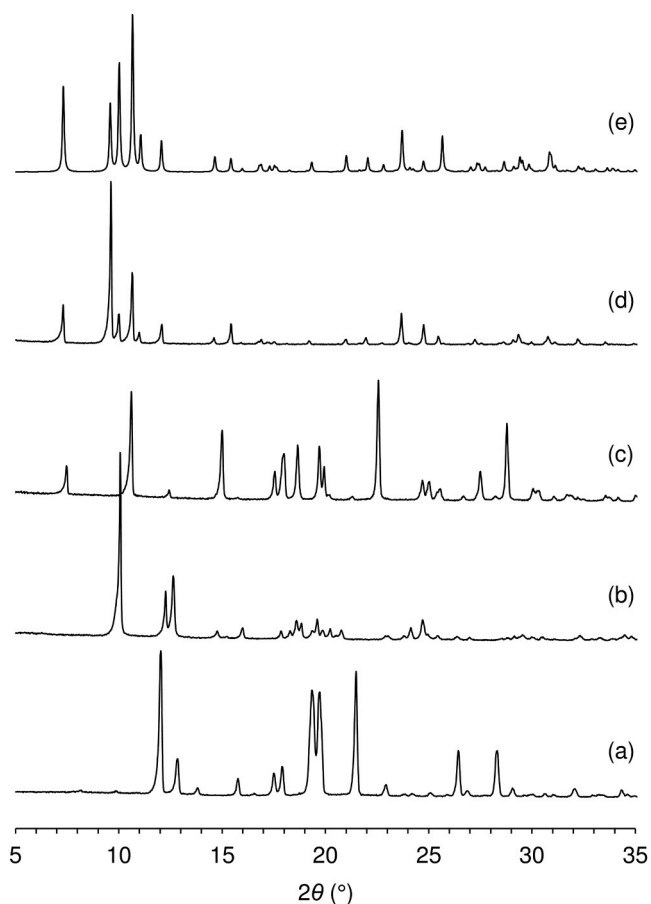


Fig. 5. Experimental (a,b,c,d) and computed (e) PXRD patterns of (a) ligand *t*Bu-ptz, (b) complex **2**, (c) [*t*Bu-Hptz]Cl, and (d,e) POM hybrid salt **3**. The program Mercury (copyright CCDC, ver. 4.0) [50] was used to generate the computed pattern from the crystal structure for **3**.

significantly to lower field upon protonation (Fig. S1 in the Supporting Information). Notably, the four signals for the [*t*Bu-Hptz]⁺ cation in **3** are shifted even further downfield relative to those in [*t*Bu-Hptz]Cl, which may be due to the influence of the hexamolybdate polyanion.

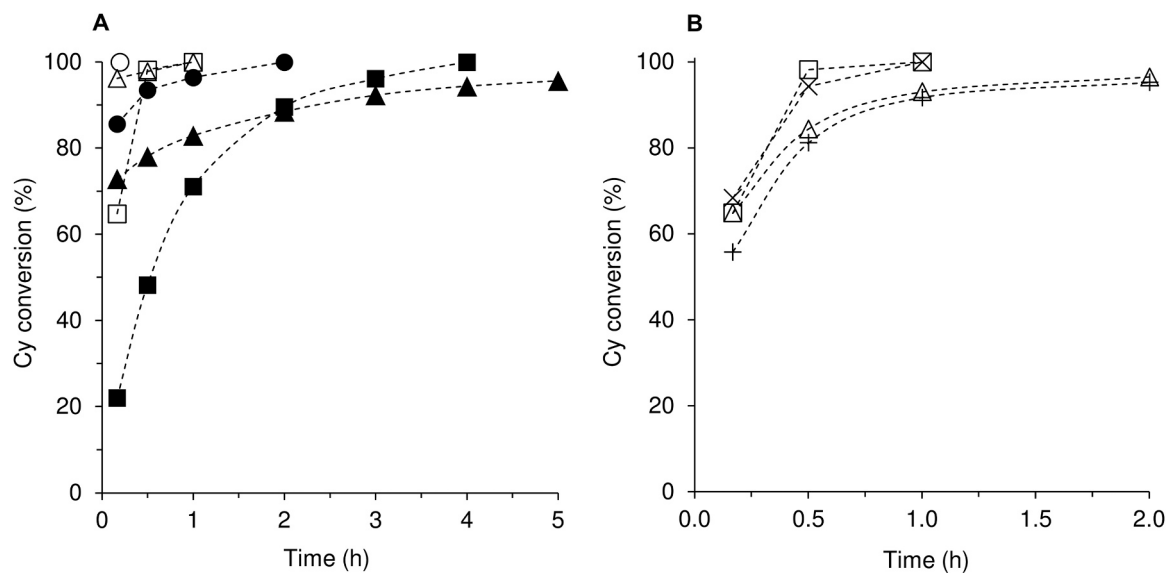


Fig. 6. *cis*-Cyclooctene epoxidation with TBHP: (A) in the presence of **1** (triangles), **2** (circles) and **3** (squares) at 55 °C (filled symbols) or 70 °C (open symbols), and (B) at 70 °C, in the presence of **3** (□), **3**-S-TBHP-run1 (×), and leaching tests (LT) for **3** (Δ) and **3**-S-TBHP-run1 (+). The dashed lines are visual guides.

The hydrolysis of **2** to give the POM hybrid salt **3** contrasts with the results obtained with the related complexes (H₂ptz)[MoO₂Cl₂(ptz)] (**1**) [33] and [MoO₂Cl₂(Hpto)] (Hpto = 5-(2-pyridyl-1-oxide)tetrazole) [51], which gave polymeric MOXI hybrid materials formulated as [MoO₃(Hpytz)] and [MoO₃(Hpto)], respectively. It seems that the *tert*-butyl substituent on the tetrazole ring in **2** has a strong structure-directing influence, leading to a POM salt in which the Hptz derivative is present as a non-coordinating counter-cation rather than (as in the hybrid from **1**) a Mo-coordinated bidentate ligand. In the next section, catalytic studies with the previously reported compound **1** and the new compounds **2** and **3** are described and compared.

3.2. Catalytic studies

3.2.1. Comparison of the performances of 1–3

The catalytic performances of **2** and **3** were firstly studied in the model epoxidation reaction of *cis*-cyclooctene (Cy) with TBHP, at 70 °C. The two catalysts were very active, leading to quantitative cyclooctene oxide (CyO) yield within 10 min or 1 h reaction for **2** and **3**, respectively (Fig. 6a). Without catalyst and/or oxidant the reaction is negligible, indicating that both catalyst and TBHP are necessary for the catalytic reaction to occur.

To compare the performances of **2** and **3** with **1**, the latter complex was tested under identical Cy/TBHP reaction conditions. Comparing the two mononuclear compounds, **2** was more active than **1**. Specifically, Cy conversion at 10 min/70 °C was 96% for **1**, and 100% for **2**, with corresponding initial TOFs of 577 and 600 mol mol_{Mo}⁻¹ h⁻¹. The difference in catalytic activity was very pronounced at the lower reaction temperature of 55 °C (Fig. 6a); for **1** and **2**, conversion at 10 min was 73% and 86%, with initial TOFs of 437 and 514 mol mol_{Mo}⁻¹ h⁻¹. PXRD patterns and ATR FT-IR spectra of the respective recovered solids (*i*-S-TBHP-run1, *i* = **1** or **2**) indicated that **1** and **2** were not stable and were converted to different types of metal species. An unknown compound or mixture of species was formed in the case of **1**, whereas **2** was converted to a POM of the type **3** (Fig. 7). These results suggest that **2** is an efficient precursor to **3** under the synthesis or catalytic reaction conditions. The epoxidation reaction was faster for **2** than for **3** (initial TOF = 600 and 389 mol mol_{Mo}⁻¹ h⁻¹, respectively), which may be because the former acts as a catalyst before being fully converted in situ, and/or the conversion of **2** to **3** may involve intermediate metal species which (depending on their lifetimes) may play catalytic roles, contributing to

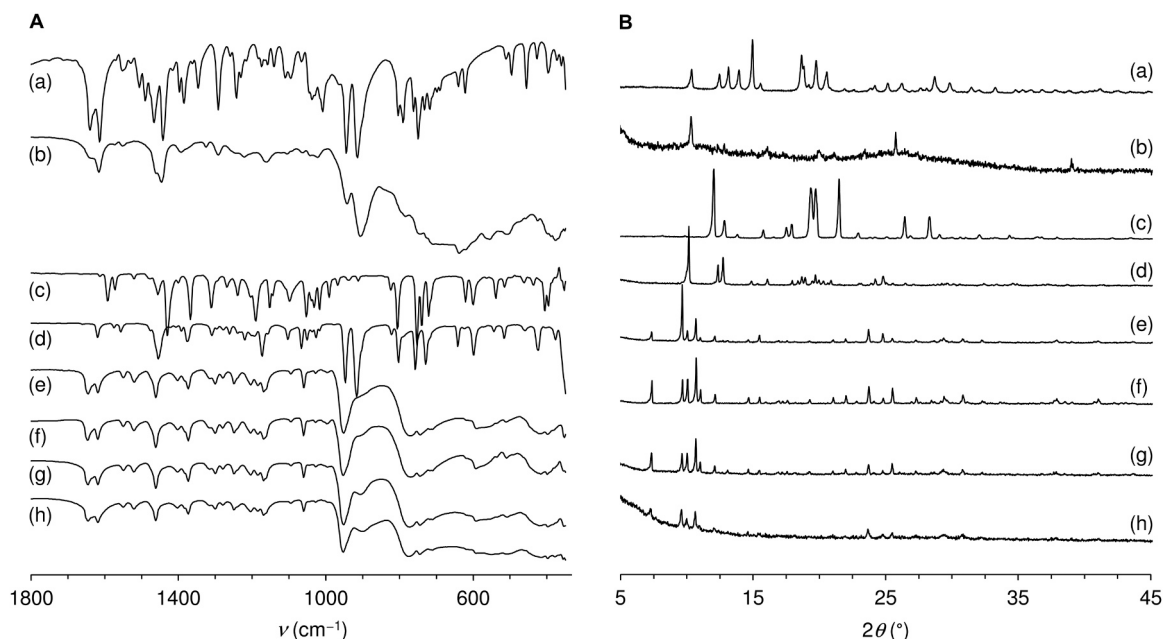


Fig. 7. ATR FT-IR spectra (A) and PXRD patterns (B) of the original and used catalysts: (a) **1**, (b) 1-S-TBHP-run1, (c) *t*Bu-ptz, (d) **2**, (e) 2-S-TBHP-run1, (f) **3**, (g) 3-S-TBHP-run1, and (h) 3-S-TBHP-run2.

the overall epoxidation reaction kinetics.

Compound **3** led to a biphasic solid-liquid reaction mixture. To check the catalytic contribution of the soluble metal species, leaching tests (LT) were carried out for the original and used catalyst (**3** and 3-S-TBHP-run1, respectively). The two LTs gave similar results, i.e., Cy conversion at 30 min/1 h (after catalyst filtration) was 84%/93% for **3** and 81%/92% for 3-S-TBHP-run1 (Fig. 6b). Although the LTs led to slightly lower conversions than those for the catalytic tests performed without catalyst filtration, these results suggest that the soluble fraction of **3** had an important catalytic contribution. The fact that the homogeneous catalytic contributions were similar for the original and used solids suggests that **3** is a stable homogeneous catalyst. In further support of this hypothesis, the use of the recovered solid 3-S-TBHP-run1 in a consecutive batch run resulted in a kinetic curve that was roughly coincident with that of the original catalyst **3** (Fig. 6b). Moreover, the PXRD patterns and ATR FT-IR spectra of the original and recovered solids were similar, i.e., the microstructure and chemical features of **3** were preserved (Fig. 7). Another advantage of **3** is that TBHP efficiency was 100% (based on iodometric titration), i.e., this catalyst did not exhibit measurable catalase-like activity, which may contribute to a minimal E-factor for the epoxidation process (mass of waste/mass of desired product).

Catalyst **3** is one of the few molybdenum-based Lindqvist-type POMs reported in the literature for catalytic epoxidation. Table 1 compares **3** to other POMs of the type [Q][Mo₆O₁₉] or [Q]₂[Mo₆O₁₉], where Q is an organic cation or a cationic organomolybdenum complex. Despite the differences in reaction conditions used, **3** outperforms the reported POMs. The POM [{MoO₂(HC(3,5-Me₂pz)₃)}₂(μ₂-O)][Mo₆O₁₉], which was tested under similar reaction conditions to those used for **3**, led to 87% Cy conversion at 24 h/55 °C (entry 8, Table 1) [52], whereas **3** led to 100% conversion at 4 h/55 °C. The reported studies, excluding one [52], did not address the critical question of catalyst stability. Catalyst **3** also outperforms a Keggin-type POM bearing a 2-(tetrazol-5-yl)pyridinium cation, namely (H₂ptz)₄[SiMo₁₂O₄₀]•*n*H₂O, which led to 84%/100% Cy conversion at 6 h/24 h (70 °C), compared to 100% at 1 h for **3** [56].

3.2.2. Influence of the amount of catalyst, type of oxidant and solvent on the performance of **3**

As discussed above, catalyst **3** led to very fast Cy reaction at 70 °C

(complete within 1 h, using initial mole ratio Mo: Cy = 1:100). On the other hand, although the catalytic reaction was homogeneous, the reaction mixture was biphasic solid-liquid, suggesting that it was saturated in **3**. Hence, the influence of the amount of catalyst on the reaction kinetics was studied, at 55 °C. Specifically, decreasing the initial Mo: Cy mole ratio from 1:100 to 0.6:100 and then to 0.2:100 (which correspond to 1, 0.6 and 0.2 mol% Mo, respectively) led to slower reaction; the initial TOF decreased in the order 132 mol mol_{Mo}⁻¹ h⁻¹ (1 mol%) > 104 mol mol_{Mo}⁻¹ h⁻¹ (0.6 mol%) > 22 mol mol_{Mo}⁻¹ h⁻¹ (0.2 mol%), and 100% conversion was reached within 4 h for 0.6–1 mol% Mo and within 6 h for 0.2 mol% Mo (in the latter case, conversion at 4 h was 97%).

The use of aqueous TBHP (TBHPaq) instead of the organic solution of TBHP at 70 °C, led to a slower reaction in the presence of **3** (63% and 100% conversion at 1 h, respectively, with BZF as solvent) (Fig. 8). These results may be partly due to mass transfer limitations since two immiscible liquid phases were obtained for TBHPaq/BZF. On the other hand, water may compete with the reactants for coordination to the metal center, retarding the overall epoxidation reaction. This hypothesis is put forward considering mechanistic studies reported in the literature for olefin epoxidation with TBHP, in the presence of molybdenum coordination compounds as catalysts. Specifically, the epoxidation reaction may be heterolytic, involving the activation of TBHP to give an active oxidizing species (e.g., a transition state possessing a moiety of the type {Mo(OH)(OOR)} with R = *tert*-butyl) which is responsible for the O-atom transfer to the olefin, leading to the epoxide product [57,58]. Accordingly, the formation of transition states involves coordination between the reactant molecules and the molybdenum species, which may be retarded in the presence of coordinating solvents such as water. Somewhat in agreement with this hypothesis is the fact that using the coordinating solvent MeCN instead of non-coordinating BZF led to a slower Cy reaction, even though the mixture Cy/TBHPaq/MeCN was completely homogeneous (22% conversion at 1 h for Cy/TBHPaq/MeCN) (Fig. 8). Employing aqueous H₂O₂ as oxidant led to similar results (19%/58% Cy conversion at 1 h/4 h) to those for TBHPaq (22%/61% conversion); for the two oxidants, the reaction mixtures were homogeneous. These results are roughly comparable with those reported in the literature for Lindqvist POM salts possessing the cation [MoO₂(HL)]⁺, where HL is a pyridoxal hydrazone derivative, but a lower amount of catalyst was used for the latter (entry 18, Table 1) [54].

Table 1Catalytic results for **3** and literature data for POMs bearing the anion $[\text{Mo}_6\text{O}_{19}]^{2-}$ and organic or organometal cations, tested as catalysts for *cis*-cyclooctene (Cy) epoxidation.

Entry	Catalyst cation ^a	Mo:Cy:ox ^b	Solv; T; ox ^c	t (h)	Conv. (%) ^d	Select. (%) ^e	Stability ^f	Ref.
1	[tBu-Hptz] ⁺	1:100:153	BZF; 55; TBHP	1/4	71/100	100/100		This work
2	[tBu-Hptz] ⁺	1:100:153	BZF; 70; TBHP	1	r1–100 r2–100	r1–100 r2–100	Stable (2 runs); similar ATR and PXRD	This work
3	[tBu-Hptz] ⁺	1:100:153	BZF; 70; TBHPaq	1/4	63/84	100/100	nr	This work
4	[tBu-Hptz] ⁺	1:100:153	MeCN; 70; TBHPaq	1/4	22/61	100/100	nr	This work
5	[tBu-Hptz] ⁺	1:100:153	MeCN; 70; H ₂ O ₂	1/4	19/58	100/100	nr	This work
6	[tBu-Hptz] ⁺	1:100:153	[BMIM]BF ₄ ; 70; TBHP	4/24	r1–92/100 r2–71/97 r3–71/98	r1–100/100 r2–100/100 r3–100/100	Steady after run 1 (3 runs)	This work
7	[tBu-Hptz] ⁺	1:100:153	[BMIM]NTf ₂ ; 70; TBHP	2/4	r1–96/100 r2–89/97 r3–86/96	r1–100/100 r2–100/100 r3–100/100	Roughly stable (3 runs)	This work
8	[{MoO ₂ (HC(3,5-Me ₂ pz) ₃) ₂ (μ ₂ -O)}] ²⁺	1:100:152	DCE; 55; TBHP	6/24	r1–46/87 r2–45/86	r1–100/100 r2–100/100	Stable (2 runs); similar ATR and PXRD	[52]
9	[(n-C ₄ H ₉) ₄ N] ⁺	1:50:100	MeCN:toluene = 3 (v/v); 55; H ₂ O ₂ or TBHP	28 (H ₂ O ₂) 3.5 (TBHP)	H ₂ O ₂ -56 TBHP-13	H ₂ O ₂ -57 TBHP-15	nr	[53]
10	[(n-C ₄ H ₉) ₄ N] ⁺	1:666:1333	-; 80; TBHPaq	6	30	53	nr	[54]
11	[(n-C ₄ H ₉) ₄ P] ⁺	1:17:33	MeCN, [BMIM]X (X = BF ₄ , NTf ₂ or PF ₆); 60; TBHP	4	MeCN-30 [BMIM]BF ₄ -9 [BMIM]NTf ₂ -56 [BMIM]PF ₆ -69	MeCN-100 [BMIM] BF ₄ -100 [BMIM]NTf ₂ -100 [BMIM]PF ₆ -100	nr	[55]
12	[(n-C ₄ H ₉) ₄ P] ⁺	1:17:33	MeOH, MeCN, [BMIM]X (X = BF ₄ , NTf ₂ or PF ₆); 60; H ₂ O ₂	4	MeOH-70 MeCN-29 [BMIM]BF ₄ -17 [BMIM]NTf ₂ -54 [BMIM]PF ₆ -49	MeOH-100 MeCN-100 [BMIM] BF ₄ -100 [BMIM]NTf ₂ -100 [BMIM]PF ₆ -100	nr	[55]
13	[(n-C ₄ H ₉) ₄ P] ⁺	1:17:33	[BMIM]X (X = BF ₄ , NTf ₂ or PF ₆); 60; UHP	2	[BMIM]BF ₄ -9 [BMIM]NTf ₂ -63 [BMIM]PF ₆ -89	[BMIM]BF ₄ -100 [BMIM]NTf ₂ -100 [BMIM]PF ₆ -100	nr	[55]
14	[(n-C ₄ H ₉) ₄ P] ⁺	1:17:33	[BMIM]PF ₆ ; 70; UHP	2	93	100	not stable (3 runs)	[55]
15	[(n-C ₄ H ₉) ₃ P(n-C ₁₄ H ₂₉)] ⁺	1:17:33	[BMIM]PF ₆ ; 70; UHP	2	90	100	nr	[55]
16	[BMIM] ⁺	1:17:33	[BMIM]PF ₆ ; 70; UHP	2	97	100	nr	[55]
17	[DBMIM] ⁺	1:17:33	[BMIM]PF ₆ ; 70; UHP	2	94	100	nr	[55]
18	[MoO ₂ (HL ¹⁻³)] ⁺	1:250:500	-; 80; TBHPaq	6	HL ¹ : 72 HL ² : 72 HL ³ : 76	HL ₁ : 58 HL ₂ : 53 HL ₃ : 55	nr	[54]

^a HC(3,5-Me₂pz)₃ = tris(3,5-dimethyl-1-pyrazolyl)methane, [(n-C₄H₉)₃P(n-C₁₄H₂₉)]⁺ = tributyl (tetradecyl)phosphonium, BMIM = 1-butyl-3-methylimidazolium, DBMIM = 1,2-dimethyl-3-butylimidazolium, HL¹ = pyridoxal isonicotinic acid hydrazone, HL² = pyridoxal benzyhydrazone, HL³ = pyridoxal 4-hydroxy benzyhydrazone; ^b Initial molybdenum:olefin:oxidant molar ratio; ^c Solv = solvent, ox = oxidant, BZF = benzotrifluoride, DCE = 1,2-dichloroethane, MeCN = acetonitrile, TBHP = decane solution of *tert*-butyl hydroperoxide, TBHPaq = aqueous solution of *tert*-butyl hydroperoxide, H₂O₂ = aqueous solution of hydrogen peroxide, UHP = urea hydrogen peroxide. ^d Conv. = Cy conversion; ri = runi (i = 1, 2 and 3). ^e Select. = CyO selectivity. ^f Stability studies, based on consecutive catalytic runs using recovered solids, and ATR FT-IR and/or PXRD of recovered solids; nr = not reported.

Using a similar initial Mo:olefin:oxidant ratio, the results for **3** (100% conversion at 24 h) are superior to those reported for (H₂ptz)₄[SiMo₁₂O₄₀]•nH₂O with TBHP/MeCN or H₂O₂/MeCN (18% and 91% Cy conversion at 24 h, respectively) [56].

3.2.3. Catalyst recycling

Since compound **3** is an ionic homogeneous catalyst, ionic liquids (ILs) are potentially suitable solvents to facilitate its recovery and reuse. To test this, [BMIM]BF₄ and [BMIM][NTf₂] were used for recycling **3**/IL mixtures at 70 °C (Fig. 9). For the two **3**/IL systems, the reaction rate decreased from run 1 to run 2, but then remained similar. Nevertheless,

for **3**/[BMIM][NTf₂], 96–100% CyO yield was reached at 4 h, and for **3**/[BMIM]BF₄, 97–100% CyO yield was reached at 24 h (Fig. 9), with corresponding total turnover numbers (TONs) of 300 and 295 mol mol⁻¹Mo, respectively. The beneficial effect of ILs possessing the anion NTf₂⁻ in relation to counterparts possessing the anion BF₄⁻, for Mo-catalyzed epoxidation with TBHP, was previously reported for the POM [(n-C₄H₉)₄P]₂[Mo₆O₁₉], tested for the Cy/TBHP reaction at 70 °C (entry 13, Table 1) [55]. In that study, the referred POM and three others, namely [Q]₂[Mo₆O₁₉] with Q = [(n-C₄H₉)₃P(n-C₁₄H₂₉)]⁺, [BMIM]⁺ or [DBMIM]⁺, were tested for Cy epoxidation with H₂O₂ (urea hydrogen peroxide (UHP)) in [BMIM]PF₆ (entries 13–17, Table 1), which led to

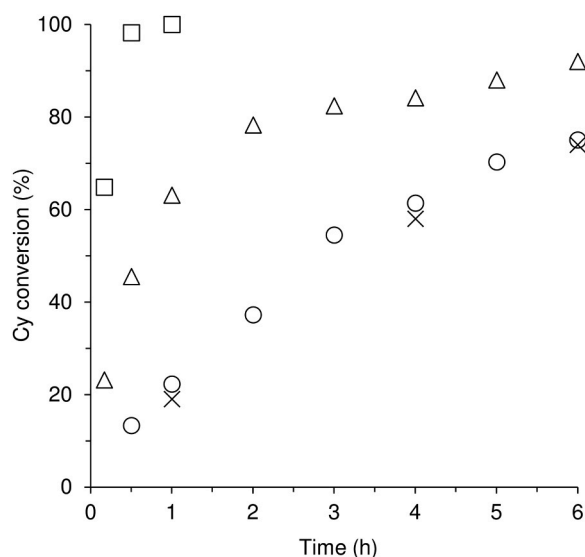


Fig. 8. Kinetic profiles for *cis*-cyclooctene epoxidation at 70 °C in the presence of **3** using the oxidant/solvent systems TBHP/BZF (□), TBHPaq/BZF (Δ), TBHPaq/MeCN (○) and H₂O₂/MeCN (×).

CyO yields of 90–97% at 2 h, although the catalyst suffered a partial drop in activity over three consecutive runs.

The fact that the Cy/TBHP reaction was faster in [BMIM][NTf₂] than in [BMIM]BF₄ suggests that the type of anion influences the reaction kinetics; conversion at 10 min/4 h was 50%/100% and 19%/92%, respectively (initial TOF = 300 and 114 mol mol_{Mo}⁻¹ h⁻¹, respectively). Besides the type of anion of the IL, other factors may affect the overall reaction kinetics. For example, the presence of water in the ILs (in different amounts) is often unavoidable, which may influence the level of hydration of the anions, the strength of the anion-cation interactions, and viscosity of the IL medium [59]. On the other hand, one cannot exclude the possibility that ion-exchange takes place between **3** and the IL to different extents, depending on the type of IL.

3.2.4. Epoxidation of bio-derived olefins

Catalyst **3** was further explored for the epoxidation of vegetable biomass-derived olefins under the optimal reaction conditions (TBHP/BZF/70 °C); specifically, methyl oleate (OLE) and methyl linoleate (LIN) as examples of FAMES, and *dl*-limonene (LIM) as an example of a terpene (Table 2, Fig. 10). These olefins may be obtained from renewable

biomass; LIN and OLE from canola, soybean and sunflower oils, LIM from citrus oils. Non-edible sources of these bioolefins include side-streams of the biodiesel (FAMES) and citrus juice (LIM) industries. Epoxidized FAMES have important applications as plasticizers, avoiding the use of petroleum-derived phthalates and their detrimental impacts on human health [60–62]. Moreover, they may be used as lubricants, detergents, coatings, and fuel additives, or as intermediates to polyurethane [61,63–65]. Limonene (di)epoxides and diols are used as solvents and fragrances, and as intermediates to pharmaceuticals, polycarbonates (replacing petroleum-derived bisphenol-A (BPA) based polycarbonates, which is desirable since BPA may be an endocrine disruptor, neurotoxic and carcinogenic agent), polyesters (via copolymerization with dicarboxylic acid anhydrides) and non-isocyanate polyurethanes [66–72].

The reaction of LIM was fast (initial TOF = 528 mol mol_{Mo}⁻¹ h⁻¹) and gave 100% LIM conversion and 100% selectivity towards 1,2-epoxy-*p*-menth-8-ene isomers (LIMOX) at 30 min/70 °C (Table 2, Fig. 10). Regarding the FAMES, OLE conversion was 97% at 3 h/70 °C, and the selectivity to the epoxide methyl 9,10-epoxyoctadecanoate was 100%. With LIN as substrate, conversion reached 85% at 24 h/70 °C, and selectivity towards total monoepoxides (methyl 12,13-epoxy-9-octadecenoate and methyl 9,10-epoxy-12-octadecenoate isomers (LINOx)) was 100% at 36% conversion (30 min). The slower reaction of LIN than of OLE (verified for **3** after 10 min reaction) has been reported previously for a related POM, (H₂ptz)₄[SiMo₁₂O₄₀]•*n*H₂O, tested under similar reaction conditions [56].

Between 30 min and 24 h of the LIN reaction, the LINOx selectivity decreased to 83%, and the total diepoxide selectivity (methyl 9,10,12,13-diepoxyoctadecanoate isomers (LINDiOx)) increased to 17% (Fig. 10). Increasing the LIN/TBHP reaction temperature from 70° to 90°C led to faster reaction kinetics (initial TOF increased from 114 to 386 mol mol_{Mo}⁻¹ h⁻¹) and 63% LINOx yield and 37% LINDiOx yield at 100% conversion, reached at 2 h. These results suggest that the overall mechanism may involve the series of reactions LIN-LINOx-LINDiOx. On the other hand, based on the kinetic profiles, LINOx may be produced as sole product by operating under ca. 60% conversion at 70 °C, and, on the other hand, LINDiOx production is favored by increasing the reaction time and/or temperature (Fig. 10).

To the best of our knowledge, compound **3** is the only [Mo₆O₁₉]²⁻ type POM tested as catalyst for OLE and LIN reactions, and [BMIM]₂[Mo₆O₁₉] is the only other hexamolybdate POM salt that has been reported as a catalyst for the epoxidation of LIM [55]. The [BMIM]⁺ salt was used in the LIM reaction with UHP and [BMIM]PF₆ as solvent, which led to 100% LIMOX selectivity at 24% conversion, 7 h/70 °C [55].

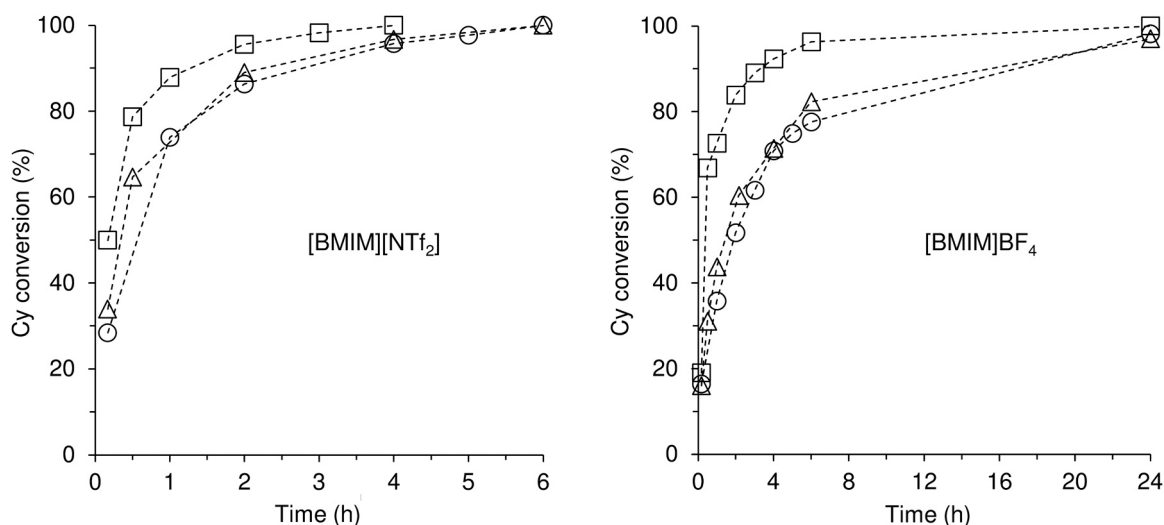
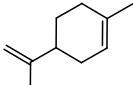
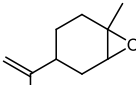
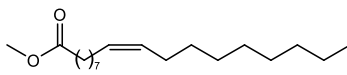
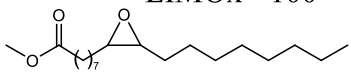
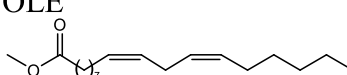
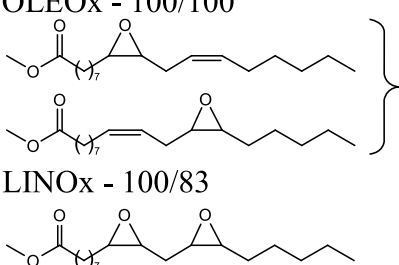


Fig. 9. Consecutive *cis*-cyclooctene epoxidation runs at 70 °C using **3**/TBHP (□-run1, Δ-run 2, ○-run 3) in the presence of [BMIM][NTf₂] and [BMIM]BF₄ as solvents.

Table 2
Epoxidation of biomass-derived olefins with **3** using TBHP as oxidant and BZF as solvent.

Olefin	T (°C); t (h)	Conv. (%)	Product selectivities (%)
 LIM	70; 0.5	100	 LIMox - 100
 OLE	70; 0.5/3	73/97	 OLEox - 100/100
 LIN	70; 0.5/24	36/85	 LINOx - 100/83 LINDiOx - 0/17
	90; 0.5/2	80/100	LINOx - 81/63 LINDiOx - 19/37

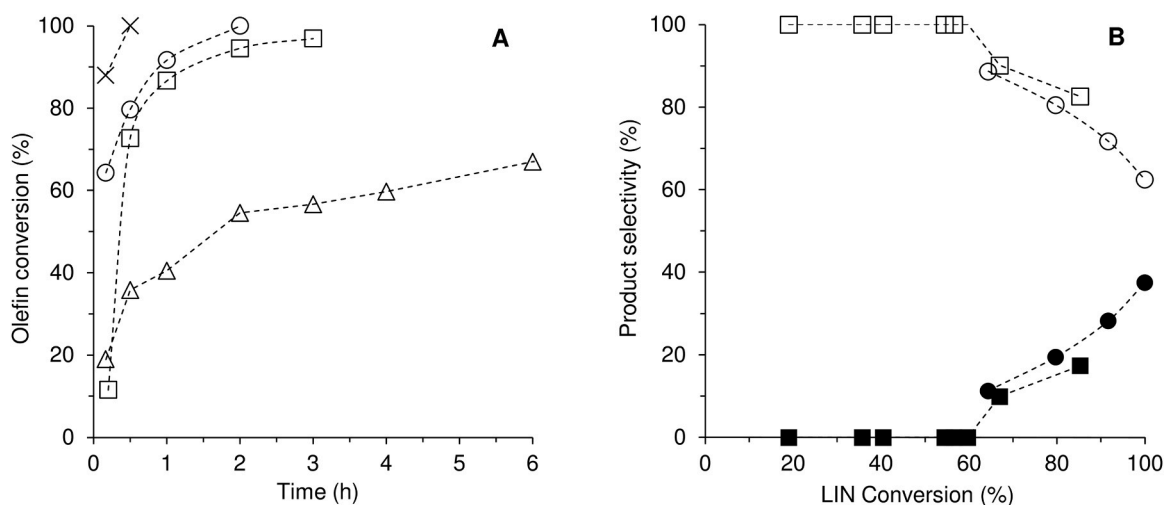


Fig. 10. (A) Kinetic profiles of the reactions of LIM (×), OLE (□) and LIN (Δ) at 70 °C, and of LIN at 90 °C (○), in the presence of **3** using TBHP as oxidant and BZF as solvent. (B) Selectivity to LINOx (□,○) and LINDiOx (■,●) as a function of LIN conversion at 70 °C (□,■) and 90 °C (○,●).

Other coordination compounds bearing 5-(2-pyridyl)-2H-tetrazole derivatives as organic components were reported in the literature for the reactions of LIM, LIN and OLE, namely (H₂ptz)₄[SiMo₁₂O₄₀]•nH₂O and the polymeric hybrid [MoO₃(Hpytz)] [33,56]. However, these catalysts were less active than **3**. Specifically, the polymeric hybrid led to 100% conversion of LIM and OLE at 24 h/70 °C, and 86% LIN conversion at 24 h/70 °C [33]; (H₂ptz)₄[SiMo₁₂O₄₀]•nH₂O led to 100% conversion of OLE and LIN at 24 h, and 85% LIM conversion at 24 h [56]. Moreover, these other catalysts, especially the silicododecamolybdate, disadvantageously led to side reactions associated with epoxide ring opening.

4. Conclusions

For the first time, compounds **2** and **3** were studied as olefin epoxidation catalysts. Subtle changes in the 5-(2-pyridyl)tetrazole ligand led to complexes possessing different chemical structures and catalytic activity. Specifically, the ligands 5-(2-pyridyl)tetrazole (Hptz) and 2-*tert*-butyl-5-(2-pyridyl)-2H-tetrazole (*t*Bu-ptz) led to ionic and neutral

dichlorodioxomolybdenum(VI) complexes, respectively. The neutral complex **2** is more active than the ionic complex **1**, based on the model reaction of *cis*-cyclooctene with TBHP, at 70 °C. Under catalytic reaction conditions, **2** is a precursor to the new polyoxometalate salt **3**. The TBHP efficiency was 100% with **3**. This POM performed as a stable homogeneous catalyst and could be recycled using an ionic liquid. The use of aqueous H₂O₂ or TBHPaq led to slower reaction kinetics.

Compound **3** is the first hexamolybdate POM salt studied for the epoxidation of the biobased FAMES methyl oleate and methyl linoleate. Succeeding the only literature study of a hexamolybdate POM salt for the catalytic epoxidation of the terpene *dl*-limonene [55], the present study shows that hexamolybdate POM salts may be designed to meet superior catalytic performances. Catalyst **3** is promising for selectively upgrading fatty acid methyl esters and terpenes to epoxides, specifically, it led to 100% *dl*-limonene conversion at 1 h, 100% methyl oleate conversion at 3 h, and 85% methyl linoleate conversion at 24 h/70 °C. Future studies of the influence of the type of cation (Q⁺) on the performances of [Q]₂[Mo₆O₁₉] type POMs may lead to new discoveries,

such as new reaction-induced self-separating metal catalysts which may be easily separated in a similar fashion to heterogeneous catalysts [73].

CRedit authorship contribution statement

Martinique S. Nunes: Investigation, Validation, Writing – original draft preparation. **Ana C. Gomes:** Investigation, Validation, Writing – original draft preparation. **Patrícia Neves:** Investigation, Validation, Writing – original draft preparation, Project administration, Funding acquisition. **Ricardo F. Mendes:** Investigation, Validation, Writing – original draft preparation. **Filipe A. Almeida Paz:** Visualization, Supervision, Writing – original draft preparation. **André D. Lopes:** Investigation, Project administration, Funding acquisition. **Martyn Pillinger:** Conceptualization, Methodology, Visualization, Supervision, Resources, Writing – review & editing, Project administration. **Isabel S. Gonçalves:** Conceptualization, Methodology, Visualization, Supervision, Resources, Writing – review & editing, Project administration. **Anabela A. Valente:** Conceptualization, Methodology, Visualization, Supervision, Resources, Writing – review & editing, Project administration.

Declaration of Competing Interest

The authors declare that they have no known competing financial interests or personal relationships that could have appeared to influence the work reported in this paper.

Data availability

Data will be made available on request.

Acknowledgments

This work was carried out with the support of CICECO - Aveiro Institute of Materials (FCT (Fundação para a Ciência e a Tecnologia, Portugal) ref. UIDB/50011/2020, UIDP/50011/2020 and LA/P/0006/2020) and the COMPETE 2020 Operational Thematic Program for Competitiveness and Internationalization (Project POCI-01-0145-FEDER-030075), co-financed by national funds through the FCT/MCTES (Portugal, PIDDAC) and the European Union through the European Regional Development Fund under the Portugal 2020 Partnership Agreement. This study received Portuguese national funds from the FCT through the operational programs CRES Algarve 2020 and COMPETE 2020 through project EMBRC.PT ALG-01-0145-FEDER-022121. M.S.N. (grant ref. 2021.06403.BD) acknowledges the FCT for Ph.D. grant (State Budget, European Social Fund (ESF) within the framework of PORTUGAL2020, namely through the Centro 2020 Regional Operational Program). A.C.G. (CEECIND/02128/2017) and R.F.M. (CEE-CIND/00553/2017) thank the FCT/MCTES for funding through the Individual Call to Scientific Employment Stimulus.

Appendix A. Supporting information

Supplementary data associated with this article can be found in the online version at [doi:10.1016/j.cattod.2023.114273](https://doi.org/10.1016/j.cattod.2023.114273).

References

- [1] K.A. Jørgensen, Transition-metal-catalyzed epoxidations, *Chem. Rev.* 89 (1989) 431–458, <https://doi.org/10.1021/cr00093a001>.
- [2] R. Sanz, M.R. Pedrosa, Applications of dioxomolybdenum(VI) complexes to organic synthesis, *Curr. Org. Chem.* 6 (2009) 239–263, <https://doi.org/10.2174/157017909788921871>.
- [3] M. Amini, M.M. Haghdoost, M. Bagherzadeh, Oxido-peroxido molybdenum(VI) complexes in catalytic and stoichiometric oxidations, in: *Coord. Chem. Rev.* 257, 2013, pp. 1093–1121, <https://doi.org/10.1016/j.ccr.2012.11.018>.
- [4] K. Jeyakumar, D.K. Chand, Application of molybdenum(VI) dichloride dioxide (MoO_2Cl_2) in organic transformations, *J. Chem. Sci.* 121 (2009) 111–123, <https://doi.org/10.1007/s12039-009-0013-z>.
- [5] R. Hernández-Ruiz, R. Sanz, Dichlorodioxomolybdenum(VI) complexes: Useful and readily available catalysts in organic synthesis, *Synthesis* 50 (2018) 4019–4036, <https://doi.org/10.1055/s-0037-1610236>.
- [6] Y. Shen, P. Jiang, P.T. Wai, Q. Gu, W. Zhang, Recent progress in application of molybdenum-based catalysts for epoxidation of alkenes, *Catalysts* 9 (2019) 31, <https://doi.org/10.3390/catal9010031>.
- [7] M. Gahagan, A. Iraqi, D.C. Cupertino, R.K. Mackie, D.J. Cole-Hamilton, A high activity molybdenum containing epoxidation catalyst and its use in regioselective epoxidation of polybutadiene, *J. Chem. Soc., Chem. Commun.* (1989) 1688–1690, <https://doi.org/10.1039/C39890001688>.
- [8] A. Iraqi, D.J. Cole-Hamilton, Preparation and reactivity of polyepoxides and polyketones: catalytic oxidation of polybutadienes, *J. Mater. Chem.* 2 (1992) 183–190, <https://doi.org/10.1039/JM9920200183>.
- [9] R. Clarke, D.J. Cole-Hamilton, The effect of added molecular sieves on alkene epoxidation reactions catalysed by $[\text{MoO}_2\text{Cl}_2\text{L}]$, where L is a 3-(diethoxyphosphoryl) derivative of camphor, *J. Chem. Soc., Dalton Trans.* (1993) 1913–1914, <https://doi.org/10.1039/DT9930001913>.
- [10] R. Clarke, M. Gahagan, R.K. Mackie, D.F. Foster, D.J. Cole-Hamilton, M. Nicol, A. W. Montford, Alkene epoxidation catalysed by camphor-derived β -ketophosphonate complexes of molybdenum(VI), *J. Chem. Soc., Dalton Trans.* (1995) 1221–1226, <https://doi.org/10.1039/DT9950001221>.
- [11] F.J. Arnaiz, R. Aguado, J.M. Martínez de Illarduya, Dioxomolybdenum(VI) halides as oxotransfer catalysts, *Polyhedron* 13 (1994) 3257–3259, [https://doi.org/10.1016/S0277-5387\(00\)83389-6](https://doi.org/10.1016/S0277-5387(00)83389-6).
- [12] H. Arzoumanian, L. Maurino, G. Agrifoglio, Thiocyanatodioxomolybdenum(VI) complexes as efficient oxidizing agents, *J. Mol. Catal. A: Chem.* 117 (1997) 471–478, [https://doi.org/10.1016/S1381-1169\(96\)00297-X](https://doi.org/10.1016/S1381-1169(96)00297-X).
- [13] K. Jeyakumar, D.K. Chand, Aerobic oxidation of benzyl alcohols by Mo^{VI} compounds, *Appl. Organomet. Chem.* 20 (2006) 840–844, <https://doi.org/10.1002/aoc.1141>.
- [14] R. Sanz, R. Aguado, M.R. Pedrosa, F.J. Arnáiz, Simple and selective oxidation of thiols to disulfides with dimethylsulfoxide catalyzed by dichlorodioxomolybdenum(VI), *Synthesis* (2002) 856–858, <https://doi.org/10.1055/s-2002-28520>.
- [15] K. Jeyakumar, D.K. Chand, Selective oxidation of sulfides to sulfoxides and sulfones at room temperature using H_2O_2 and a Mo(VI) salt as catalyst, *Tetrahedron Lett.* 47 (2006) 4573–4576, <https://doi.org/10.1016/j.tetlet.2006.04.153>.
- [16] D. Julião, A.C. Gomes, M. Pillinger, R. Valença, J.C. Ribeiro, I.S. Gonçalves, S. S. Balula, A recyclable ionic liquid-oxomolybdenum(VI) catalytic system for the oxidative desulfurization of model and real diesel fuel, *Dalton Trans.* 45 (2016) 15242–15248, <https://doi.org/10.1039/c6dt02065h>.
- [17] D. Julião, A.C. Gomes, L. Cunha-Silva, M. Pillinger, A.D. Lopes, R. Valença, J. C. Ribeiro, I.S. Gonçalves, S.S. Balula, Dichlorodioxomolybdenum(VI) complexes bearing oxygen-donor ligands as catalysts for oxidative desulfurization of simulated and real diesel, *Catal. Commun.* 128 (2019), 105704, <https://doi.org/10.1016/j.catcom.2019.05.011>.
- [18] D. Julião, A.C. Gomes, M. Pillinger, A.D. Lopes, R. Valença, J.C. Ribeiro, I. S. Gonçalves, S.S. Balula, Desulfurization of diesel by extraction coupled with Mo-catalyzed sulfoxidation in polyethylene glycol-based deep eutectic solvents, *J. Mol. Liq.* 309 (2020), 113093, <https://doi.org/10.1016/j.molliq.2020.113093>.
- [19] D. Julião, A.C. Gomes, L. Cunha-Silva, M. Pillinger, I.S. Gonçalves, S.S. Balula, Dichloro and dimethyl dioxomolybdenum(VI)-bipyridine complexes as catalysts for oxidative desulfurization of dibenzothiophene derivatives under extractive conditions, *J. Organomet. Chem.* 967 (2022), 122336, <https://doi.org/10.1016/j.jorganchem.2022.122336>.
- [20] F.E. Kühn, E. Herdtweck, J.J. Haider, W.A. Herrmann, I.S. Gonçalves, A.D. Lopes, C.C. Romão, Bis-acetonitrile(dibromo)dioxomolybdenum(VI) and derivatives: synthesis, reactivity, structures and catalytic applications, *J. Organomet. Chem.* 583 (1999) 3, [https://doi.org/10.1016/S0022-328X\(99\)00102-3](https://doi.org/10.1016/S0022-328X(99)00102-3).
- [21] F.E. Kühn, A.D. Lopes, A.M. Santos, E. Herdtweck, J.J. Haider, C.C. Romão, A. G. Santos, Lewis base adducts of bis-(halogeno)dioxomolybdenum(VI): syntheses, structures, and catalytic applications, *J. Mol. Catal. A: Chem.* 151 (2000) 147–160, [https://doi.org/10.1016/S1381-1169\(99\)00262-9](https://doi.org/10.1016/S1381-1169(99)00262-9).
- [22] F.E. Kühn, A.M. Santos, A.D. Lopes, I.S. Gonçalves, E. Herdtweck, C.C. Romão, (Dimethyl)dioxomolybdenum(VI) complexes: syntheses and catalytic applications, *J. Mol. Catal. A: Chem.* 164 (2000) 25–38, [https://doi.org/10.1016/S1381-1169\(00\)00200-4](https://doi.org/10.1016/S1381-1169(00)00200-4).
- [23] F.E. Kühn, M. Groarke, É. Benze, E. Herdtweck, A. Prazeres, A.M. Santos, M. J. Calhorda, C.C. Romão, I.S. Gonçalves, A.D. Lopes, M. Pillinger, Octahedral Bipyridine and Bipyrimidine Dioxomolybdenum(VI) Complexes: Characterization, Application in Catalytic Epoxidation, and Density Functional Mechanistic Study, *Chem. Eur. J.* 8 (2002) 2370–2383, [10.1002/1521-3765\(20020517\)8:10%3C2370::AID-CHEM2370%3E3.0.CO;2-A](https://doi.org/10.1002/1521-3765(20020517)8:10%3C2370::AID-CHEM2370%3E3.0.CO;2-A).
- [24] F.E. Kühn, A.M. Santos, A.D. Lopes, I.S. Gonçalves, J.E. Rodríguez-Borges, M. Pillinger, C.C. Romão, Chiral bis(oxazoline) and pyridyl alcoholate dioxomolybdenum(VI) complexes: synthesis, characterization and catalytic examinations, *J. Organomet. Chem.* 621 (2001) 207–217, [https://doi.org/10.1016/S0022-328X\(00\)00774-9](https://doi.org/10.1016/S0022-328X(00)00774-9).
- [25] A. Günyar, D. Betz, M. Drees, E. Herdtweck, F.E. Kühn, Highly soluble dichloro, dibromo and dimethyl dioxomolybdenum(VI)-bipyridine complexes as catalysts for the epoxidation of olefins, *J. Mol. Catal. A: Chem.* 331 (2010) 117–124, <https://doi.org/10.1016/j.molcata.2010.08.014>.

- [26] M. Abrantes, T.R. Amarante, M.M. Antunes, S. Gago, F.A.A. Paz, I. Margiolaki, A. E. Rodrigues, M. Pillinger, A.A. Valente, I.S. Gonçalves, Synthesis, structure, and catalytic performance in cyclooctene epoxidation of a molybdenum oxide/bipyridine hybrid material: $\{[\text{MoO}_3(\text{bipy})][\text{MoO}_3(\text{H}_2\text{O})]_n\}$, *Inorg. Chem.* 49 (2010) 6865–6873, <https://doi.org/10.1021/ic100479a>.
- [27] T.R. Amarante, P. Neves, A.C. Gomes, M.M. Nolasco, P. Ribeiro-Claro, A.C. Coelho, A.A. Valente, F.A.A. Paz, S. Smeets, L.B. McCusker, M. Pillinger, I.S. Gonçalves, Synthesis, Structural elucidation, and catalytic properties in olefin epoxidation of the polymeric hybrid material $[\text{Mo}_3\text{O}_9(2\text{-}[\text{3}(5\text{-pyrazolyl})\text{pyridine}])_n]$, *Inorg. Chem.* 53 (2014) 2652–2665, <https://doi.org/10.1021/ic403033j>.
- [28] S.M. Bruno, C.C.L. Pereira, M.S. Balula, M. Nolasco, A.A. Valente, A. Hazell, M. Pillinger, P. Ribeiro-Claro, I.S. Gonçalves, New chloro and triphenylsiloxy derivatives of dioxomolybdenum(VI) chelated with pyrazolylpyridine ligands: Catalytic applications in olefin epoxidation, *J. Mol. Catal. A: Chem.* 261 (2007) 79–87, <https://doi.org/10.1016/j.molcata.2006.07.064>.
- [29] T.R. Amarante, P. Neves, C. Tomé, M. Abrantes, A.A. Valente, F.A.A. Paz, M. Pillinger, I.S. Gonçalves, An octanuclear molybdenum(VI) complex containing coordinatively bound 4,4'-di-*tert*-butyl-2,2'-bipyridine, $[\text{Mo}_8\text{O}_{22}(\text{OH})_4(\text{di-}t\text{-Bu-bipy})_4]$: Synthesis, structure, and catalytic epoxidation of bio-derived olefins, *Inorg. Chem.* 51 (2012) 3666–3676, <https://doi.org/10.1021/ic202640a>.
- [30] S. Figueiredo, A.C. Gomes, P. Neves, T.R. Amarante, F.A.A. Paz, R. Soares, A. D. Lopes, A.A. Valente, M. Pillinger, I.S. Gonçalves, Synthesis, structural elucidation, and application of a pyrazolylpyridine–molybdenum oxide composite as a heterogeneous catalyst for olefin epoxidation, *Inorg. Chem.* 51 (2012) 8629–8635, <https://doi.org/10.1021/ic301405r>.
- [31] M. Abrantes, I.S. Gonçalves, M. Pillinger, C. Vurchio, F.M. Cordero, A. Brandi, Molybdenum oxide/bipyridine hybrid material $\{[\text{MoO}_3(\text{bipy})][\text{MoO}_3(\text{H}_2\text{O})]_n\}$ as catalyst for the oxidation of secondary amines to nitrones, *Tetrahedron Lett.* 52 (2011) 7079–7082, <https://doi.org/10.1016/j.tetlet.2011.10.079>.
- [32] D. Julião, A.C. Gomes, M. Pillinger, I.S. Gonçalves, S.S. Balula, Desulfurization and denitrogenation processes to treat diesel using Mo(VI)-bipyridine catalysts, *Chem. Eng. Technol.* 43 (2020) 1774–1783, <https://doi.org/10.1002/ceat.201900624>.
- [33] M.S. Nunes, D.M. Gomes, A.C. Gomes, P. Neves, R.F. Mendes, F.A.A. Paz, A. D. Lopes, A.A. Valente, I.S. Gonçalves, M. Pillinger, A 5-(2-pyridyl)tetrazolate complex of molybdenum(VI), its Structure, and transformation to a molybdenum oxide-based hybrid heterogeneous catalyst for the epoxidation of olefins, *Catalysts* 11 (2021) 1407, <https://doi.org/10.3390/catal11111407>.
- [34] A.P. Mosalkova, S.V. Voitekhovich, A.S. Lyakhov, L.S. Ivashkevich, J. Lach, B. Kersting, P.N. Gaponik, O.A. Ivashkevich, 2-*tert*-Butyl-5-(2-pyridyl)-2H-tetrazole as a chelating ligand in the direct synthesis of novel Cu(II) and heterobimetallic Cu(II)/Mn(II) complexes, *Dalton Trans.* 42 (2013) 2985–2997, <https://doi.org/10.1039/C2DT32512H>.
- [35] E. Ocansey, J. Darkwa, B.C.E. Makhubela, Iridium and palladium CO_2 hydrogenation in water by catalyst precursors with electron-rich tetrazole ligands, *Organometallics* 39 (2020) 3088–3098, <https://doi.org/10.1021/acs.organomet.0c00276>.
- [36] O.G. Shakirova, L.G. Lavrenova, N.V. Kuratieva, A.S. Bogomyakov, L. A. Sheludyakova, A.P. Mosalkova, Y.V. Grigoriev, Study of the complexes of iron (II) dicyanamide and isothiocyanate with 2-(2-*tert*-butyltetrazol-5-yl)pyridine, *J. Struct. Chem.* 58 (2017) 919–925, <https://doi.org/10.1134/S0022476617050092>.
- [37] T. Kottke, D. Stalke, Crystal handling at low temperatures, *J. Appl. Crystallogr.* 26 (1993) 615–619, <https://doi.org/10.1107/S0021889893002018>.
- [38] APEX3 Crystallography Software Suite, version 2016.9–0, Bruker AXS Inc., Delft, The Netherlands, 2005–2016.
- [39] Cryopad, Remote Monitoring and Control, version 1.451, Oxford Cryosystems, Oxford, UK, 2006.
- [40] SAINT+ Data Integration Engine, version 8.37A, Bruker AXS Inc., Madison, WI, USA, 2015.
- [41] L. Krause, R. Herbst-Irmer, G.M. Sheldrick, D. Stalke, Comparison of silver and molybdenum microfocus X-ray sources for single-crystal structure determination, *J. Appl. Crystallogr.* 48 (2015) 3–10, <https://doi.org/10.1107/S1600576714022985>.
- [42] G.M. Sheldrick, SHELXT - Integrated space-group and crystal-structure determination, *Acta Crystallogr. A Found. Adv.* 71 (2015) 3–8, <https://doi.org/10.1107/S2053273314026370>.
- [43] C.B. Hübschle, G.M. Sheldrick, B. Dittrich, ShelXle: A Qt graphical user interface for SHELXL, *J. Appl. Crystallogr.* 44 (2011) 1281–1284, <https://doi.org/10.1107/S0021889811043202>.
- [44] H. Putz, K. Brandenburg, *Diamond - Crystal and Molecular Structure Visualization, version 3.2f*, Cryst. Impact GbR, Bonn., Ger. (2010).
- [45] A.C. Coelho, M. Nolasco, S.S. Balula, M.M. Antunes, C.C.L. Pereira, F.A.A. Paz, A. A. Valente, M. Pillinger, P. Ribeiro-Claro, J. Klinowski, I.S. Gonçalves, Chemistry and catalytic activity of molybdenum(VI)-pyrazolylpyridine complexes in olefin epoxidation. Crystal structures of monomeric dioxo, dioxo- μ -oxo, and oxidiperoxo derivatives, *Inorg. Chem.* 50 (2011) 525–538, <https://doi.org/10.1021/ic101384p>.
- [46] M.M. Degtyarik, P.N. Gaponik, V.V. Naumenko, A.I. Lesnikovich, M.V. Nikanovich, Infrared spectroscopic study of copper(II) complexes with *N*-substituted tetrazoles, *Spectrochim. Acta* 43A (1987) 349–353, [https://doi.org/10.1016/0584-8539\(87\)80116-2](https://doi.org/10.1016/0584-8539(87)80116-2).
- [47] A.P. Mosalkova, S.V. Voitekhovich, A.S. Lyakhov, L.S. Ivashkevich, P.N. Gaponik, O.A. Ivashkevich, Direct synthesis and characterization of new copper(II) and zinc (II) 5-*R*-tetrazolato complexes $[\text{R} = \text{Me}, \text{Ph}, 4\text{-Py}]$ with ethylenediamine and DMSO as coligands, *Z. Anorg. Allg. Chem.* 638 (2012) 103–110, <https://doi.org/10.1002/zaac.201100407>.
- [48] R.J. Abraham, J.J. Byrne, L. Griffiths, M. Perez, ^1H chemical shifts in NMR: Part 23, the effect of dimethyl sulphoxide versus chloroform solvent on ^1H chemical shifts, *Magn. Reson. Chem.* 44 (2006) 491–509, <https://doi.org/10.1002/mrc.1747>.
- [49] A.J. Bridgeman, G. Cavigliasso, Density functional study of the vibrational frequencies of Lindqvist polyanions, *Chem. Phys.* 279 (2002) 143–159, [https://doi.org/10.1016/S0301-0104\(02\)00450-0](https://doi.org/10.1016/S0301-0104(02)00450-0).
- [50] C.F. Macrae, I. Sovago, S.J. Cottrell, P.T.A. Galek, P. McCabe, E. Pidcock, M. Platings, G.P. Shields, J.S. Stevens, M. Towler, P.A. Wood, Mercury 4.0: from visualization to analysis, design and prediction, *J. Appl. Crystallogr.* 53 (2020) 226–235, <https://doi.org/10.1107/S1600576719014092>.
- [51] M.S. Nunes, D.M. Gomes, A.C. Gomes, P. Neves, R.F. Mendes, F.A.A. Paz, A. D. Lopes, M. Pillinger, A.A. Valente, I.S. Gonçalves, A Molybdenum(VI) complex of 5-(2-pyridyl-1-oxide)tetrazole: Synthesis, structure, and transformation into a MoO₃-based hybrid catalyst for the epoxidation of bio-olefins, *Catalysts* 13 (2023) 565, <https://doi.org/10.3390/catal13030565>.
- [52] A.C. Gomes, P. Neves, S. Figueiredo, J.A. Fernandes, A.A. Valente, F.A.A. Paz, M. Pillinger, A.D. Lopes, I.S. Gonçalves, Tris(pyrazolyl)methane molybdenum tricarbonyl complexes as catalyst precursors for olefin epoxidation, *J. Mol. Catal. A: Chem.* 370 (2013) 64–76, <https://doi.org/10.1016/j.molcata.2012.12.010>.
- [53] C. Bhaumik, E. Manoury, J.-C. Daran, P. Sözen-Aktaş, F. Demirhan, R. Poli, Investigation of the reaction of $[\text{Cp}^*\text{M}_2\text{O}_5]$ (M = Mo, W) with hydrogen peroxide and *tert*-butylhydroperoxide in MeCN; implications for olefin epoxidation catalyzed by organomolybdenum and organotungsten compounds, *J. Organomet. Chem.* 760 (2014) 115–123, <https://doi.org/10.1016/j.jorganchem.2013.11.029>.
- [54] J. Pisk, B. Prugovečki, D. Matković-Čalogović, T. Jednačak, P. Novak, D. Agustin, V. Vrdoljak, Pyridoxal hydrazoneato molybdenum(VI) complexes: Assembly, structure and epoxidation (pre)catalyst testing under solvent-free conditions, *RSC Adv.* 4 (2014) 39000–39010, <https://doi.org/10.1039/c4ra08179j>.
- [55] B. Zhang, S. Li, A. Pöthig, M. Cokoja, S.-L. Zang, W.A. Herrmann, F.E. Kühn, Oxidation reactions catalyzed by polyoxomolybdate salts, *Z. Naturforsch. B* 68 (2013) 587–597, <https://doi.org/10.5560/ZNB.2013-3033>.
- [56] P. Neves, A.C. Gomes, L. Cunha-silva, A.A. Valente, M. Pillinger, I.S. Gonçalves, A silicododecamolybdate/pyridinium-tetrazole hybrid molecular salt as a catalyst for the epoxidation of bio-derived olefins, *Inorg. Chim. Acta* 516 (2021), 120129, <https://doi.org/10.1016/j.ica.2020.120129>.
- [57] A. Al-Ajlouni, A.A. Valente, C.D. Nunes, M. Pillinger, A.M. Santos, J. Zhao, C. C. Romão, I.S. Gonçalves, F.E. Kühn, Kinetics of cyclooctene epoxidation with *tert*-butyl hydroperoxide in the presence of $[\text{MoO}_2\text{X}_2\text{L}]$ -type catalysts (L = bidentate Lewis base), *Eur. J. Inorg. Chem.* (2005) 1716–1723, <https://doi.org/10.1002/ejic.200400852>.
- [58] L.F. Veiros, A. Prazeres, P.J. Costa, C.C. Romão, F.E. Kühn, M.J. Calhorda, Olefin epoxidation with *tert*-butyl hydroperoxide catalyzed by $\text{MoO}_2\text{X}_2\text{L}$ complexes: a DFT mechanistic study, *Dalton Trans.* (2006) 1383–1389, <https://doi.org/10.1039/b515484g>.
- [59] C. Ma, A. Laaksonen, C. Liu, X. Lu, X. Ji, The peculiar effect of water on ionic liquids and deep eutectic solvents, *Chem. Soc. Rev.* 47 (2018) 8685–8720, <https://doi.org/10.1039/c8cs00325d>.
- [60] W. He, G. Zhu, Y. Gao, H. Wu, Z. Fang, K. Guo, Green plasticizers derived from epoxidized soybean oil for poly(vinyl chloride): Continuous synthesis and evaluation in PVC films, *Chem. Eng. J.* 380 (2020), 122532, <https://doi.org/10.1016/j.cej.2019.122532>.
- [61] H. Hosney, B. Nadiem, I. Ashour, I. Mustafa, A. El-Shibiny, Epoxidized vegetable oil and bio-based materials as PVC plasticizer, *J. Appl. Polym. Sci.* 135 (2018) 46270, <https://doi.org/10.1002/app.46270>.
- [62] <https://www.cargill.com/page/epoxides> (consulted on 29/03/2023).
- [63] K.M. Doll, S.Z. Erhan, Synthesis and performance of surfactants based on epoxidized methyl oleate and glycerol, *J. Surfactants Deterg.* 9 (2006) 377–383, <https://doi.org/10.1007/s11743-006-5016-x>.
- [64] N.B. Samartha, P.A. Mahanwar, Modified vegetable oil based additives as a future polymeric material—Review, *Open J. Org. Polym. Mater.* 5 (2015) 1–22, <https://doi.org/10.4236/ojopm.2015.51001>.
- [65] Y. Li, X. Luo, S. Hu, Polyols and polyurethanes from vegetable oils and their derivatives, in: *Bio-based polyols and polyurethanes*, 2015, pp. 15–43, SpringerBriefs in Molecular Science, Springer, Cham, https://doi.org/10.1007/978-3-319-21539-6_2.
- [66] N. Mahato, K. Sharma, M. Sinha, E.R. Baral, R. Koteswararao, A. Dhyan, M. Hwan Cho, S. Cho, Bio-sorbents, industrially important chemicals and novel materials from citrus processing waste as a sustainable and renewable bioresource: A review, *J. Adv. Res* 23 (2020) 61–82, <https://doi.org/10.1016/j.jare.2020.01.007>.
- [67] F. Parrino, A. Fidalgo, L. Palmisano, L.M. Ilharco, M. Pagliaro, R. Ciriminna, Polymers of limonene oxide and carbon dioxide: Polycarbonates of the solar economy, *ACS Omega* 3 (2018) 4884–4890, <https://doi.org/10.1021/acsomega.8b00644>.
- [68] O. Hauenstein, M. Reiter, S. Agarwal, B. Rieger, A. Greiner, Bio-based polycarbonate from limonene oxide and CO_2 with high molecular weight, excellent thermal resistance, hardness and transparency, *Green. Chem.* 18 (2016) 760–770, <https://doi.org/10.1039/c5gc01694k>.
- [69] P.A. Wilbon, F. Chu, C. Tang, Progress in renewable polymers from natural terpenes, terpenoids, and rosin, *Macromol. Rapid Commun.* 34 (2013) 8–37, <https://doi.org/10.1002/marc.201200513>.
- [70] A. Corma, S. Iborra, A. Velty, Chemical routes for the transformation of biomass into chemicals, *Chem. Rev.* 107 (2007) 2411–2502, <https://doi.org/10.1021/cr050989d>.
- [71] S.G. Leitão, G.R. Martins, L. Martínez-Fructuoso, D.D.S. Silva, T.S. da Fonseca, C.V. V. Castilho, L.C. Baratto, D.S. Alviano, C.S. Alviano, G.G. Leitão, R. Pereda-Miranda, Absolute stereochemistry of antifungal limonene-1,2-diols from *Lippia*

- rubella*, Rev. Bras. Farmacogn. 30 (2020) 537–543, <https://doi.org/10.1007/s43450-020-00081-x>.
- [72] P. Gallezot, Catalytic routes from renewables to fine chemicals, Catal. Today 121 (2007) 76–91, <https://doi.org/10.1016/j.cattod.2006.11.019>.
- [73] P. Neves, D.M. Gomes, I.S. Gonçalves, M. Pillinger, A.A. Valente, Reaction induced self-separating metal catalysts – Wonder Systems in 21st Century Catalysis, Coord. Chem. Rev. 491 (2023), 215229, <https://doi.org/10.1016/j.ccr.2023.215229>.